

The darkening of the
Greenland ice sheet

M. Tedesco et al.

Title Page

Abstract

Introduction

Conclusions

References

Tables

Figures



Back

Close

Full Screen / Esc

Printer-friendly Version

Interactive Discussion



The darkening of the Greenland ice sheet: trends, drivers and projections (1981–2100)

M. Tedesco^{1,2,3}, S. Doherty⁴, X. Fettweis⁵, P. Alexander^{1,2,6}, J. Jeyaratnam¹,
E. Noble¹, and J. Stroeve⁷

¹The City College of New York – CUNY, New York, USA

²The Graduate Center of the City University of New York, New York, USA

³Lamont Doherty Earth Observatory of Columbia University, New York, NY, USA

⁴Joint Institute for the Study of the Atmosphere and Ocean (JISAO), University of Washington,
Seattle, WA, USA

⁵University of Liege, Liege, Belgium

⁶NASA Goddard Institute for Space Studies, New York, NY, USA

⁷University of Boulder, Colorado, USA

Received: 6 September 2015 – Accepted: 15 September 2015 – Published: 19 October 2015

Correspondence to: M. Tedesco (cryocity@gmail.com)

Published by Copernicus Publications on behalf of the European Geosciences Union.

Abstract

The surface energy balance and meltwater production of the Greenland ice sheet (GrIS) are modulated by snow and ice albedo through the amount of absorbed solar radiation. Here we show, using spaceborne multispectral data collected during the three decades from 1981 to 2012, that summertime surface albedo over the GrIS decreased at a statistically significant (99%) rate of 0.02 decade^{-1} between 1996 and 2012. The negative trend is confined to the regions of the GrIS that undergo melting in summer with the dry-snow zone showing no trend. The period 1981–1996 showed no statistically significant trend. The analysis of the outputs of a regional climate model indicates that the drivers of the observed albedo decrease is imputable to a combination of increased near-surface temperatures, which enhanced melt and promoted growth in snow grain size and the expansion of bare ice areas, as well as by trends in light-absorbing impurities on the snow and ice surfaces. Neither aerosol models nor in situ observations indicate increasing trends in impurities in the atmosphere over Greenland, suggesting that their apparent increase in snow and ice might be related to the exposure of a “dark band” of dirty ice and to the consolidation of impurities at the surface with melt. Albedo projections through the end of the century under different warming scenarios consistently point to continued darkening, with albedo anomalies in 2100 averaged over the whole ice sheet lower than in 2000 by 0.08, driven solely by a warming climate. Future darkening is likely underestimated because of known underestimates in projected melting and because the model albedo scheme does not currently include light-absorbing impurities and the effect of biological activity, which themselves have a positive feedback, leading to increased melting, grain growth and darkening.

The darkening of the Greenland ice sheet

M. Tedesco et al.

Title Page

Abstract

Introduction

Conclusions

References

Tables

Figures



Back

Close

Full Screen / Esc

Printer-friendly Version

Interactive Discussion



1 Introduction

The summer season over the Greenland ice sheet (GrIS) during the past two decades has been characterized by increased surface melting (Nghiem et al., 2012; Tedesco et al., 2011, 2014) and net mass loss (Shepherd et al., 2012). Notably, the summer of 2012 set new records for surface melt extent (Nghiem et al., 2012) and duration (Tedesco et al., 2013), and a record of 570 ± 100 Gt in total mass loss, doubling the average annual loss rate of 260 ± 100 Gt for the period 2003–2012 (Tedesco et al., 2014).

Net solar radiation is the most significant driver of summer surface melt over the GrIS (van den Broeke et al., 2011; Tedesco et al., 2011), and is determined by the combination of the amount of incoming solar radiation and surface albedo. Variations in snow albedo are driven principally by changes in snow grain size and by the presence of light-absorbing impurities (hereafter, simply “impurities”, e.g., Warren and Wiscombe, 1982). Generally, snow albedo is highest immediately following new snowfall. In the normal course of *destructive metamorphism* the snow grains become rounded, and large grains grow at the expense of small grains, so the average grain radius r increases with time (LaChapelle, 1969). Subsequently, warming and melt/freeze cycles catalyse grain growth, decreasing albedo mostly in the near-infrared (NIR) region (Warren, 1982). The absorbed solar radiation associated with this albedo reduction promotes additional grain growth, further reducing albedo, potentially accelerating melting. The presence of impurities such as soot (black carbon, BC), dust, organic matter, algae and other biological material in snow or ice also reduces the albedo, mostly in the visible and ultraviolet regions (Warren, 1982). Such impurities are deposited through dry and wet deposition, and their mixing ratios are enhanced through snow water loss in sublimation and melting (Conway et al., 1996; Flanner et al., 2007; Doherty et al., 2013). Besides grain growth and impurities, another cause of albedo reduction over the GrIS is the exposure of bare ice: once layers of snow or firn are removed through ablation, the exposure of the underlying bare ice will further reduce

TCD

9, 5595–5645, 2015

The darkening of the Greenland ice sheet

M. Tedesco et al.

Title Page

Abstract

Introduction

Conclusions

References

Tables

Figures



Back

Close

Full Screen / Esc

Printer-friendly Version

Interactive Discussion



surface albedo, as does the presence of melt pools on the ice surface (e.g., Tedesco et al., 2011).

Most of the studies examining albedo over the whole GrIS have focused on data collected by the Moderate Resolution Imaging Spectroradiometer (MODIS) starting in 2000 (e.g., Box et al., 2012; Tedesco et al., 2013). At the same time, regional climate models (RCMs) have been employed to simulate the evolution and trends of surface quantities over the GrIS back to the 1960s using reanalysis data for forcing (e.g., Fettweis et al., 2012). Despite the increased complexity of models, and their inclusion of increasingly sophisticated physics parameterizations, RCMs still suffer from incomplete representation of processes that drive snow albedo changes, such as the spatial and temporal distribution of impurities and from the absence of in situ grain size measurement to validate models describing the evolution of snow grains. In this study, we first report the results of the analysis of summer spaceborne albedo estimates over the whole GrIS for the period 1980–2012, hence expanding the temporal coverage with respect to previous studies. Then, we combine the outputs of a RCM and in situ observations with the albedo spaceborne estimates to identify those processes responsible for the observed albedo trends. The model, Modèle Atmosphérique Régionale (MAR), is used to simulate surface temperature, exposed ice area, and surface albedo over Greenland at large spatial scales. MAR-simulated surface albedo is tested against surface albedo retrieved under the Global Land Surface Satellite (GLASS) project, and it is used to attribute trends in GLASS albedo. Lastly, we project the evolution of mean summer albedo over Greenland by using the MAR model forced with the outputs of different Earth System Models (ESMs) under different CO₂ scenarios. Discussions and conclusions follow the presentation of the methods and results.

TC D

9, 5595–5645, 2015

The darkening of the Greenland ice sheet

M. Tedesco et al.

Title Page

Abstract

Introduction

Conclusions

References

Tables

Figures



Back

Close

Full Screen / Esc

Printer-friendly Version

Interactive Discussion



2 Methods and data

2.1 The MAR regional climate model and its albedo scheme

5 Simulations of surface energy balance quantities over the GrIS are performed using the Modèle Atmosphérique Régionale (MAR; e.g., Fettweis et al., 2005, 2013). MAR is a modular atmospheric model that uses the sigma-vertical coordinate to simulate
10 airflow over complex terrain and the Soil Ice Snow Vegetation Atmosphere Transfer scheme (SISVAT; e.g., De Ridder and Gallée, 1998) as the surface model. MAR outputs have been assessed over Greenland in several studies (e.g., Tedesco et al., 2011; Fettweis et al., 2005; Vernon et al., 2013; Rae et al., 2012; Van Angelen et al., 2012), with recent work specifically focusing on assessing simulated albedo
15 over Greenland (Alexander et al., 2014). The snow model in MAR, is the CROCUS model of Brun et al. (1992), which calculates albedo for snow and ice as a function of snow grain properties, being in turn dependent on energy and mass fluxes within the snowpack. The model configuration used here has 25 terrain-following sigma layers
20 between the Earth's surface and the 5 hPa-model top. The spatial configuration of the model uses the 25 km horizontal resolution computational domain over Greenland described in Fettweis et al. (2005). The lateral and lower boundary conditions are prescribed from meteorological fields modelled by the global European Centre for Medium-Range Weather Forecasts (ECMWF) Interim Reanalysis (ERA-Interim, <http://www.ecmwf.int/en/research/climate-reanalysis/era-interim>). Sea-surface temperature and sea-ice cover are also prescribed in the model using the same reanalysis data. The atmospheric model within MAR interacts with the CROCUS model, which provides the state of the snowpack and associated quantities (e.g., albedo, grain size). No nudging or interactive nesting was used in any of the experiments.

25 The MAR albedo scheme is summarized below. Surface albedo is expressed as a function of the optical properties of snow, the presence of bare ice, whether snow is overlying ice (and whether the surface is waterlogged), and the presence of clouds. In the version used here (MAR v3.5.1), the broadband albedo (α_s , 0.3–2.8 μm) of snow

The darkening of the Greenland ice sheet

M. Tedesco et al.

Title Page

Abstract

Introduction

Conclusions

References

Tables

Figures



Back

Close

Full Screen / Esc

Printer-friendly Version

Interactive Discussion



is a weighted average (Eq. 1) of the albedo in three spectral bands, α_1 , α_2 and α_3 , which are functions of the optical diameter of snow grains (d , in m), as modified from equations by Brun et al. (1992); e.g., Lefebvre et al. (2003); Alexander et al. (2014):

$$\alpha_s = 0.58\alpha_1 + 0.32\alpha_2 + 0.10\alpha_3 \quad (1)$$

$$\alpha_1 = \max(0.94, 0.96 - 1.58\sqrt{d}), \quad (0.3\text{--}0.8\ \mu\text{m}) \quad (2)$$

$$\alpha_2 = 0.95 - 15.4\sqrt{d}, \quad (0.8\text{--}1.5\ \mu\text{m}) \quad (3)$$

$$\alpha_3 = 364 \cdot \min(d, 0.0023) - 32.31\sqrt{d} + 0.88, \quad (1.5\text{--}2.8\ \mu\text{m}) \quad (4)$$

The optical diameter d is, in turn, a function of snow grain properties and it evolves as described in Brun et al. (1992). In MAR, the albedo of snow is calculated by Eqs. (1)–(4), but it is not permitted to drop below 0.65.

For the transition from snow to ice, MAR makes the albedo an explicit function of density. On a polar ice sheet, densification of snow/firn/ice occurs in three stages, with a different physical process responsible for the densification in each stage (Herron and Langway, 1980; Arnaud et al., 2000). Newly-fallen snow can have density in the range 50–200 kg m⁻³. The snow densifies over time by *grain-boundary sliding*, attaining a maximum density of 550 kg m⁻³ at the surface. Old melting snow at the surface in late summer typically has this density, but does not exceed it, because this is the maximum density that can be attained by grain-boundary sliding and corresponds to the density of random-packing of spheres (Benson, 1962, p. 77). Further increases of density (the second stage) occur in *firn* under the weight of overlying snow, by *grain deformation* (pressure-sintering). In this case the density range is 550–830 kg m⁻³. At a density of 830 kg m⁻³ the air becomes closed off into bubbles and the material is called *ice*. In the third stage, the density of ice increases from 830 to 917 kg m⁻³ by shrinkage of air bubbles under pressure. Moving down the slope along the surface of the GrIS, at the transition

between the accumulation area and the ablation area, the snow melts away, exposing firn. Continuing farther down, the firn melts away, exposing ice. The albedo of firn may

The darkening of the Greenland ice sheet

M. Tedesco et al.

Title Page

Abstract

Introduction

Conclusions

References

Tables

Figures



Back

Close

Full Screen / Esc

Printer-friendly Version

Interactive Discussion



be approximated as a function of its density ρ , interpolating between the minimum albedo of snow and the maximum albedo of ice. In MAR these values of albedo are set to 0.65 and 0.55, respectively. We would then have for the density range of firn (550–830 kg m⁻³):

$$\alpha_{\text{firn}} = 0.55 + (0.65 - 0.55)(830 - \rho)/(830 - 550) \quad (5)$$

The MAR v3.5.1 version used here maintains a minimum albedo of 0.65 for any density up to 830 kg m⁻³, and specifies the gradual transition from snow albedo to ice albedo across the density range 830–920 kg m⁻³. This means that the albedo of exposed firn is not allowed to drop below 0.65, with the result that the positive feedbacks of snow/firn/ice albedo will be muted in MAR. This aspect is being addressed in future versions of MAR (MAR v3.6) and a sensitivity analysis is being conducted to evaluate the impact of the changes on the albedo values when snow is transitioning from firn to ice. Such analysis is computationally expensive and preliminary outputs will be published once available.

In MAR, the albedo for bare ice is a function of the accumulated surface meltwater preceding runoff and specified minimum ($\alpha_{i,\text{min}}$) and maximum ($\alpha_{i,\text{max}}$) bare ice values:

$$\alpha_i = \alpha_{i,\text{min}} + (\alpha_{i,\text{max}} - \alpha_{i,\text{min}})e^{(-M_{\text{SW}(t)}/K)} \quad (6)$$

Here $\alpha_{i,\text{min}}$ and $\alpha_{i,\text{max}}$ are set, respectively, to 0.4 and 0.55, K is a scale factor set to 200 kg m⁻², and $M_{\text{SW}(t)}$ is the time-dependent accumulated excess surface meltwater before runoff (in kg m⁻²).

When a snowpack with depth less than 10 cm is overlying a layer with a density exceeding 830 kg m⁻³ (i.e., ice), the albedo in MAR is a weighted, vertically-averaged value of snow albedo (α_S) and ice albedo (α_I). When the snowpack depth exceeds 10 cm, the value is set to α_S . The presence of clouds can increase snow albedo because they absorb at the same NIR wavelengths where snow also absorbs, skewing the incident solar spectrum to wavelengths for which snow has higher albedo (Fig. 5 of

The darkening of the Greenland ice sheet

M. Tedesco et al.

Title Page

Abstract

Introduction

Conclusions

References

Tables

Figures



Back

Close

Full Screen / Esc

Printer-friendly Version

Interactive Discussion



Grenfell et al., 1981; Fig. 13 of Warren, 1982; Greuell and Konzelman, 1994), in which case the albedos of snow and ice are adjusted based on the cloud fraction modelled by MAR.

2.2 The GLASS albedo product

The GLASS surface albedo product (<http://glcf.umd.edu/data/abd/>) is derived from the combination of data collected by the Advanced Very High Resolution Radiometer (AVHRR) and the MODerate resolution Imaging Spectroradiometer (MODIS, Liang et al., 2013). Shortwave broadband albedo (0.3–3 μm) is provided every 8 days at a spatial resolution of 0.05° (~ 56 km in latitude) for the period 1981–2012. GLASS albedo data with a resolution of 1 km is also available from 2000 to 2012 but it is not used here for consistency with the data available before 2000. Several efforts have been made to make the AVHRR and MODIS albedo products consistent within the GLASS product, including the use of the same surface albedo spectra to train the regression and the use of a temporal filter and climatological background data to fill data gaps (Liang et al., 2013). Monthly averaged broadband albedos from GLASS-AVHRR and GLASS-MODIS were cross-compared over Greenland for those months when there was overlap (July 2000, 2003, and 2004), revealing consistency in GLASS retrieved albedo from the two sensors (He et al., 2013).

The GLASS product provides both black-sky (i.e., albedo in the absence of a diffuse component of the incident radiation) and white-sky albedo (albedo in the absence of a direct component, with an isotropic diffuse component). The actual albedo is a value interpolated between these two according to the fraction of diffuse sunlight, which is a function of the aerosol optical depth (AOD) and cloud cover fraction. In the absence of the full information needed to properly re-construct the actual albedo, here we use in our analysis the black-sky albedo, because we focus mostly on albedo retrieved under clear-sky conditions. Our analysis using the white-sky albedo (not shown here) is fully consistent with the results obtained using the black-sky albedo and reported in the following. A full description of the GLASS retrieval process and available products can

The darkening of the Greenland ice sheet

M. Tedesco et al.

Title Page

Abstract

Introduction

Conclusions

References

Tables

Figures



Back

Close

Full Screen / Esc

Printer-friendly Version

Interactive Discussion



be found in Liang et al. (2013) and references therein. An assessment of the GLASS product complementing existing studies is reported below.

Data collected by the MODIS TERRA and AQUA sensors are used in the GLASS albedo retrieval for the period 2000–2012 (2000–2012 for TERRA and 2002–2012 for AQUA, respectively). Wang et al. (2012) have shown that the MODIS TERRA sensor has been degrading at a pace that can be approximated by a second order polynomial, with the coefficients being spectrally dependent. Over Greenland, the impact of sensor degradation on albedo trends has been estimated at $-0.0059 \text{ decade}^{-1}$ (Stroeve et al., 2013). We complemented previous assessments of the MODIS and GLASS and evaluated the absolute accuracy of the GLASS retrievals by comparing monthly GLASS albedo to in situ measurements of albedo collected at automatic weather stations of the Greenland climate network (GC-Net, Steffen and Box, 2001). GC-Net data are distributed at hourly temporal resolution and were temporally averaged to match the temporal window used in the GLASS product data. The root mean square error (RMSE), percentage RMSE (pRMSE), and the slope of a linear fit between GLASS and in situ measured albedos for 12 stations are given in Table 1. The number of available years used for the statistics is also reported for each station. We considered only stations for which at least 10 years were available for the analysis in at least one of the months. Our results are consistent with the findings reported by Alexander et al. (2014) and Stroeve et al. (2013, 2006) concerning the assessment of the MODIS albedo products over the GrIS. The mean value of the RMSE for all stations is 0.04–0.05 in all months, with individual station values as high as 0.15 for station JAR1 in August and as low as 0.01 for Summit and Saddle stations in June. The relatively large RMSE value for JAR1 (and other stations located within the ablation zone) is probably due to heterogeneity of albedo values within the pixel containing the location of the station and to the point-scale nature of the in situ observations. At Summit, where spatial inhomogeneity on the surface is small, it is reasonable to assume that the effect of spatial scale and heterogeneity on the comparison is smaller.

The darkening of the Greenland ice sheet

M. Tedesco et al.

Title Page

Abstract

Introduction

Conclusions

References

Tables

Figures



Back

Close

Full Screen / Esc

Printer-friendly Version

Interactive Discussion



3 Results

3.1 Albedo trends

The time series of the mean summer GLASS albedo values between 1981 and 2012 over Greenland can be separated into two distinct periods (Fig. 1a): the period 1981–1996, when albedo shows no trend and a second period, 1996–2012, when a statistically significant trend (99%) is detected. The year 1996 was identified as the one showing the highest value of the coefficient of determination when fitting the albedo timeseries with two linear functions using a variable breaking point.

The GLASS albedo shows significant darkening ($p < 0.01$) of the surface of the GrIS for the 1996–2012 period, with the summer (JJA) albedo declining at a rate of $0.02 \pm 0.004 \text{ decade}^{-1}$ (Fig. 1a). Over the same period, MAR-simulated summer near-surface temperature increased at a rate of $0.74 \pm 0.5 \text{ }^\circ\text{C decade}^{-1}$ (Fig. 1b, $p < 0.05$), consistent with observed enhanced surface melting (e.g., Fettweis et al., 2013). MAR simulations also point to positive trends between 1996 and 2012 in summer surface grain radius ($0.12 \pm 0.03 \text{ mm decade}^{-1}$, $p < 0.01$, Fig. 1c) and the extent of those regions where bare ice is exposed during summer ($380 \pm 190 \text{ km}^2 \text{ decade}^{-1}$, $p < 0.01$, Fig. 1d). There is no statistically significant trend in GLASS albedo or MAR-simulated surface grain size and bare ice extent for the 1981–1996 period. Simulated summer snowfall (not plotted in the figure) does not show a statistically significant trend for the period 1996–2012 ($p < 0.1$, $-1702 \pm 790 \text{ mmWE decade}^{-1}$). Notably, strong negative summer snowfall anomalies from 2010 to 2012 are simulated by MAR, down to -1.5 standard deviations below the 1981–2012 mean. We suggest that for 2010–2012, reduced summer snowfall might have played a key role in the accelerated decline in albedo.

The darkening of the Greenland ice sheet

M. Tedesco et al.

Title Page

Abstract

Introduction

Conclusions

References

Tables

Figures



Back

Close

Full Screen / Esc

Printer-friendly Version

Interactive Discussion



3.2 Drivers: surface grain size and bare ice

Inter-annual variability in the mean summer GLASS albedo is captured by the MAR albedo simulations (Fig. 1a). For the period when the darkening has been identified, MAR albedo values explain $\sim 90\%$ (de-trended) of the spaceborne-derived albedo interannual variability. A multi-linear regression analysis indicates that, over the same period, the interannual variability of summer values of surface grain size and bare ice extent simulated by MAR explain, respectively, 54% (grain size) and 65% (bare ice) of the inter-annual variability of GLASS albedo when considered separately. When linearly combined, grain size, bare ice extent and snowfall explain $\sim 85\%$ of the GLASS inter-annual variability, with the influence of summer new snowfall alone explaining only 44% of the GLASS albedo variability.

The spatial distribution of observed albedo trends from space shows that the largest trends (in magnitude) occur over those regions where surface temperature, grain size, and bare ice exposure have also changed the most (Fig. 2). In particular, darkening observed from space is most pronounced at lower elevations in southwest Greenland, with trends values as low as $-0.20 \pm 0.07 \text{ decade}^{-1}$ (Fig. 2a; note that the colour bar only goes down to $-0.06 \text{ decade}^{-1}$ for graphical purposes), where trends in the number of days when simulated surface temperature exceeds 0°C (Fig. 2b), grain size (Fig. 2c) and the number of summer days when bare ice is exposed (Fig. 2d) are the largest.

While MAR is able to capture a large component of the observed variability in albedo retrieved by GLASS, the simulated albedo trend is smaller in magnitude than that estimated using the GLASS product. The largest differences occur along the southwest margin of the ice sheet (Fig. 3), where a “dark band” of outcropping layers of ice containing large concentrations of impurities is known to be present on the surface (Wientjes et al., 2011). In this region the number of days when surface temperature exceeds 0°C has increased, with trends up to more than 20 days decade^{-1} along the margins of the GrIS (Fig. 1b). During this time-period GLASS albedo values are as low as 0.30, lower than that of bare ice (i.e., 0.45), consistent with in situ measured

TC D

9, 5595–5645, 2015

The darkening of the Greenland ice sheet

M. Tedesco et al.

Title Page

Abstract

Introduction

Conclusions

References

Tables

Figures



Back

Close

Full Screen / Esc

Printer-friendly Version

Interactive Discussion



values of dirty ice (Wientjes et al., 2010; Bøggild et al., 2010). Figure 4 shows the spatial distribution of MAR and GLASS mean JJA albedo for year 2010 over an area centred on the dark band in southwest Greenland, as well as the time series of GLASS albedo averaged over the same ice-covered area contained within the region identified by the black rectangle in Fig. 4a. The black line in Fig. 4c shows the GLASS spatially-averaged albedo within this region, with the top and the bottom margins of the grey area indicating, respectively, the maximum and minimum albedo values within that area. Note that we included only pixels that contained 100% ice in all years (i.e. coloured areas in Fig. 4a and b) in the calculation shown in Fig. 4c, so trends are not driven by exposure of underlying land surface. Mean summer albedo from GLASS decreased over this area between 2005 and 2012 from ~ 0.6 to ~ 0.45 . Minimum albedo across all years averaged over the region is ~ 0.4 , but dips close to ~ 0.3 in 2010, a value consistent with dirty bare ice, as shown in previous studies (Wientjes et al., 2010, 2011; Bøggild et al., 2010). We hypothesise that the discrepancy along this dark band between MAR- and GLASS albedo values is likely due to trends in the concentrations of impurities in the snow and ice in this region, which are not currently captured by the model. This hypothesis is supported by previous studies such as the one by Wientjes et al. (2011), arguing that increased deposition of dust to this region of the ice sheet has significantly decreased the albedo.

3.3 Drivers: light-absorbing impurities on the surface of the GrIS

MAR simulations of albedo in different spectral bands (see Eqs. 1–4) point to comparable trends in the visible ($0.3\text{--}0.8\ \mu\text{m}$; $-0.009 \pm 0.005\ \text{decade}^{-1}$, $p < 0.05$) and near-infrared ($0.8\text{--}1.5\ \mu\text{m}$; $-0.010 \pm 0.004\ \text{decade}^{-1}$, $p < 0.05$) bands (Fig. 5a) and to a much smaller and not statistically significant trend in the shortwave infrared band ($1.5\text{--}2.8\ \mu\text{m}$, $-0.003 \pm 0.004\ \text{decade}^{-1}$, $p > 0.1$). Because the GLASS product does not provide visible albedo (but only broadband albedo), we extrapolated an estimate of the visible component of the GLASS albedo by subtracting the NIR and shortwave infrared albedo values computed with MAR from the GLASS broadband values, following the

The darkening of the Greenland ice sheet

M. Tedesco et al.

Title Page

Abstract

Introduction

Conclusions

References

Tables

Figures



Back

Close

Full Screen / Esc

Printer-friendly Version

Interactive Discussion



MAR albedo scheme (Eq. 1, Fig. 5b). To evaluate the robustness of this approach, we compared anomalies (with respect to year 2000) in estimated GLASS visible albedo with those from the 16 day MODIS MCD43A3 product (Stroeve et al., 2013), which also has a visible albedo product (Fig. 5b). The MODIS albedo product we used is distributed by Boston University (<https://lpdaac.usgs.gov/>) and makes use of all atmospherically-corrected MODIS reflectance measurements over 16 day periods, to provide an averaged albedo every 8 days. A semi-empirical bidirectional reflectance distribution function (BRDF) model is used to compute bi-hemispherical reflectance from these reflectance measurements (Schaaf et al., 2002). The comparison between the GLASS- and MODIS-retrieved visible albedo anomalies is shown in Fig. 5b, indicating that the two visible albedo anomalies are highly consistent, with a mean absolute error of 0.01 and a standard deviation of 0.005. There are differences in the estimated summer albedo trends from MCD43A3 and GLASS over the 2002–2012 period, with the former being $-0.04 \pm 0.001 \text{ decade}^{-1}$ and the latter $-0.03 \pm 0.008 \text{ decade}^{-1}$. This difference could be due to the method we applied to estimate the visible component of the GLASS albedo, as well as other factors related to the data processing and algorithms used to extract albedo. Notably, however, the GLASS and MCD43 visible albedo trends are consistently about twice that estimated from the MAR model. Because the MAR model does not account for the presence of surface impurities in the albedo scheme, we suggest that the underestimated darkening by MAR relative to GLASS is consistent with an increase in the concentration of surface impurities. The concentrations of impurities in surface snow and ice can increase either because of increased atmospheric deposition or because of post-depositional processes, including (a) loss of snow water to sublimation and melt, resulting in impurities accumulating at the surface as a lag-deposit (e.g., Doherty et al., 2013), and (b) the outcropping of “dirty” underlying ice associated with snow/firn removal due to ablation. These processes are themselves driven by warming, and therefore constitute positive feedbacks.

The darkening of the Greenland ice sheet

M. Tedesco et al.

Title Page

Abstract

Introduction

Conclusions

References

Tables

Figures



Back

Close

Full Screen / Esc

Printer-friendly Version

Interactive Discussion



The darkening of the Greenland ice sheet

M. Tedesco et al.

Title Page

Abstract

Introduction

Conclusions

References

Tables

Figures

◀

▶

◀

▶

Back

Close

Full Screen / Esc

Printer-friendly Version

Interactive Discussion



Quantifying the contribution of surface impurities to GLASS albedo trends is a challenging task because of the relatively low impurity concentrations over most of the GrIS (Doherty et al., 2010; Bond et al., 2013), and because of known limitations related to remote sensing estimates of impurities from space (Warren, 2013). Moreover, quantifying the causes of increased impurity concentrations on the surface (atmospheric deposition vs. other factors) is also challenging, if not prohibitive, given the current state-of-the-art of spaceborne measurements (e.g. accuracy of the satellite products) and the scarcity of in situ data. Therefore, in the next section, we focus on assessing whether atmospheric aerosol levels over the GrIS have increased (as a proxy for whether the deposition of aerosol has increased) and we look for trends in forest fires in the two of the main source regions for aerosols over the GrIS.

3.4 Attributions: atmospheric deposition of impurities and number of forest fires

3.4.1 Atmospheric deposition of impurities

Ice core analyses of black carbon in the central regions of the GrIS have been used to study long-term variability and trends in pollution deposition (McConnell et al., 2007; Keegan et al., 2014). These records show that snow at these locations was significantly more polluted in the first half of the 20th century than presently. Both these records and in situ measurements at Summit (Cachier and Pertuisot, 1994; Chylek et al., 1995; Hagler et al., 2007; Doherty et al., 2010) also indicate that in recent decades, the snow in central Greenland has been relatively clean, with concentrations smaller than 4 ngg^{-1} for BC. This amount of BC could lower snow albedo by only 0.002 for $r = 100 \mu\text{m}$, or 0.005 for $r = 500 \mu\text{m}$ (Fig. 5a of Dang et al., 2015). Black carbon in snow has also been measured in situ at single points in time at a few other locations; the only region where we can study trends is in the percolation zone of South Greenland. Snow sampled in 1983 at Dye-3 had a median of 2 ngg^{-1} (Clarke and Noone, 1985).

In 2008 and 2010, measurements 160 km away at Dye-2, using the same method, had medians of 4 ngg^{-1} in spring and 1 ngg^{-1} in summer (Table 9 of Doherty et al., 2010).

In the absence of in situ measurements of impurity concentrations over Greenland, we investigate trends in Atmospheric Optical Depth (AOD) from outputs of aerosol models and from ground-based measurements at several locations around the GrIS. AOD is a measure of the total extinction (omni-directional scattering plus absorption) of sunlight as it passes through the atmosphere, and is related to atmospheric aerosol abundance. Thus, it is a metric for the mass of aerosol available to be potentially deposited onto the GrIS surface. In the aerosol models, we are able to examine trends in total AOD as well as in aerosol components: BC, dust and organic matter. In addition, we examined trends in modelled deposition fluxes of these species to the GrIS.

For our analysis, we used model results from the Aerosol Comparisons between Observations and Models (AeroCom) project, an open international initiative aimed at understanding the global aerosol and its impact on climate (Samset et al., 2014; Myhre et al., 2013; Jiao et al., 2014; Tsigaridis et al., 2014). The project combines a large number of observations and outputs from fourteen global models to test, document and compare state-of-the-art modelling of the global aerosol. We specifically show standardised (i.e., subtracting the mean and then dividing by the standard deviation) deposition fluxes of BC, dust and organic aerosols (OA) from the GISS modelE contribution to the AeroCom phase II series of model runs (<http://aerocom.met.no/aerocomhome.html>). The runs used here took as input the decadal emission data from the Coupled Model Intercomparison Project Phase 5 (CMIP5). Figures 6 and 7 show modelled deposition fluxes at the two locations of Kangerlussuaq (Fig. 6, $67^{\circ}00'31''$ N, $50^{\circ}41'21''$ W) and Summit (Fig. 7, $72^{\circ}34'47''$ N, $38^{\circ}27'33''$ W) for the months of June, July and August and aerosol components (BC, dust and organic matter). These locations were selected as representative of the ablation zone (Kangerlussuaq) and the dry-snow zone (Summit). The analysis of the AeroCom outputs shows no statistically significant trend in the modelled fluxes for either location. Results of the analysis of fluxes over different areas point to similar conclusions. Similar results

The darkening of the Greenland ice sheet

M. Tedesco et al.

Title Page

Abstract

Introduction

Conclusions

References

Tables

Figures



Back

Close

Full Screen / Esc

Printer-friendly Version

Interactive Discussion



The darkening of the Greenland ice sheet

M. Tedesco et al.

Title Page

Abstract

Introduction

Conclusions

References

Tables

Figures



Back

Close

Full Screen / Esc

Printer-friendly Version

Interactive Discussion



are obtained when considering the months of January, February and March, when aerosol concentration is expected to be higher. The results here presented complement other studies (e.g. Stone et al., 2014) indicating that, since the 1980s, atmospheric concentrations of BC measured at surface stations in the Arctic have decreased, with variations attributed to changes in both anthropogenic and natural aerosol and aerosol precursor emissions.

Mean summer values of AOD (550 nm) measured at three AERONET (<http://aeronet.gsfc.nasa.gov>) Greenland sites based in Thule (northwest Greenland; 77°28′00″ N, 69°13′50″ W), Ittoqqortoormiit (east-central Greenland; 70°29′07″ N, 21°58′00″ W), and Kangerlussuaq during the period 2007–2013 (with the starting year ranging between 2007 and 2009, depending on the site) are reported in Table 2, together with their standard deviations. None of the stations show statistically significant trends in AOD, consistently with the results of the analysis of the modelled deposition fluxes.

A recent study (Dumont et al., 2014) concluded that dust deposition has been increasing over much of the GrIS and that this is driving lowered albedo across the ice sheet. That conclusion was based on trends of an “impurity index”, which is the ratio of the logarithm of albedo in the 545–565 nm MODIS band (where impurities affect albedo) to the logarithm of albedo in the 841–876 nm band (where they do not). In the MODIS product used in Dumont et al. (2014) study, albedo values rely on removal of the effects of aerosols in the atmosphere. In the Dumont et al. (2014) study this correction was made using simulations of atmospheric aerosols by the Monitoring Atmospheric Composition and Climate (MACC) model. Their resulting “impurity index” shows positive trends, and these are attributed in part (up to 30 %) to increases in atmospheric aerosol not accounted for by the model, and the remainder to increases in snow impurities. The latter is consistent with our findings herein: that GrIS darkening is in part attributable to an increase in the impurity content of surface snow. However, Dumont et al. (2014) assume that this increase in surface snow impurities is a result of enhanced deposition from the atmosphere. They do not account for the possibility that positive trends in impurity content may instead be a result of a warming-driven

the visible albedo over Greenland is probably not due to an increase in the rate of deposition of impurities from the atmosphere.

4 Albedo projections through 2100

We estimated future projections of albedo over the GrIS using MAR forced with the outputs of three different Earth System Models (ESMs) from CMIP5 driven by two radiative forcing scenarios (Meinshausen et al., 2011) over the 120 year period 1980–2100. The first scenario corresponds to an increase in the atmospheric greenhouse gas concentration to a level of 850 ppm CO₂ equivalent (RCP45); the second scenario increases CO₂ equivalent to > 1370 ppm in 2100 (RCP85) (Moss et al., 2010; Meinshausen et al., 2011). The three ESMs used are the second generation of the Canadian Earth System Model (CanESM2), the Norwegian Community Earth System Model (NorESM1) and the Model for Interdisciplinary Research on Climate (MIROC5) of the University of Tokyo, Japan. More information is available in Tedesco and Fettweis (2012). The ESMs are used to generate MAR outputs for the historical period (1980–2005) and for future projections (2005–2100). The Canadian Earth System Model (CanESM2, e.g. Arora and Boer, 2010; Chylek et al., 2011) combines the fourth generation climate model (CanCM4) from the Canadian Center for Climate Modelling and Analysis with the terrestrial carbon cycle based on the Canadian Terrestrial Ecosystem Model (CTEM), which models the land–atmosphere carbon exchange. The NorESM1 model is built under the structure of the Community Earth System Model (CESM) of the National Center for Atmospheric Research (NCAR). The major difference from the standard CESM configuration concerns a modification to the treatment of atmospheric chemistry, aerosols, and clouds (Seland et al., 2008) and the ocean component. Lastly, MIROC5 is a coupled general circulation model developed at the Center for Climate System Research (CCSR) of the University of Tokyo, composed of the CCSR/NIES (National Institute of Environmental Studies) atmospheric general circulation model (AGCM 5.5) and the CCSR Ocean Component Model, including

The darkening of the Greenland ice sheet

M. Tedesco et al.

Title Page

Abstract

Introduction

Conclusions

References

Tables

Figures



Back

Close

Full Screen / Esc

Printer-friendly Version

Interactive Discussion



5 a dynamic-thermodynamic sea-ice model (e.g., Watanabe et al., 2010, 2011). We refer to Tedesco and Fettweis (2012) for the evaluation of the outputs of MAR when forced with the outputs of the ESMS during the historical period (1980–2005). All simulations consistently point to darkening accelerating through the end of the century (Fig. 9), with albedo anomalies (relative to year 2000) as large as -0.08 by the end of the century over the whole ice sheet, and even more (-0.1) over the western portion of the ice sheet (Fig. 10). The magnitude of the projected albedo anomalies by 2100, however, is probably underestimated by our simulations, because (a) the model tends to underestimate melting when forced with the ESMS (Fettweis et al., 2013), and therefore underestimates grain size growth, and (b) the model currently does not account for the presence of impurities on the ice surface and for the enhanced mixing ratios in the surface of melting snow.

5 Discussion

15 Our results indicate that a darkening of the GrIS associated with increasing temperatures and enhanced melting occurred between 1996 and 2012, promoted by increased surface snow grain size, by the expansion and persistency of the areas of exposed bare ice, and by the increased surface snow impurity concentrations. We find no evidence for general increases in the deposition of impurities across the GrIS, so we associate the higher surface snow impurity concentrations predominantly with the appearance of underlying dirty ice and the consolidation of impurities in surface snow resulting from snow melt. Inter-annual variability in the JJA GLASS albedo is captured by the MAR albedo simulations, with the latter explaining $\sim 90\%$ of the spaceborne-derived albedo interannual variations for the period 1996–2012. The strong correlation between MAR and GLASS albedo time series for this period suggests that MAR is capturing the processes driving most of the albedo inter-annual variability (grain size metamorphism and bare ice exposure) and that these processes have more influence than those associated with the spatial and temporal variability of surface impurity

The darkening of the Greenland ice sheet

M. Tedesco et al.

Title Page

Abstract

Introduction

Conclusions

References

Tables

Figures



Back

Close

Full Screen / Esc

Printer-friendly Version

Interactive Discussion



The darkening of the Greenland ice sheet

M. Tedesco et al.

Title Page

Abstract

Introduction

Conclusions

References

Tables

Figures



Back

Close

Full Screen / Esc

Printer-friendly Version

Interactive Discussion



concentrations at seasonal timescales (currently not included in the MAR albedo scheme). This is plausible also in view of the relatively large impact on albedo due to grain size metamorphism by comparison to the expected albedo decrease associated with the impurity concentrations measured over the GrIS. As pointed out by Tedesco et al. (2015), for pure snow, grain growth from new snow (with $r = 100 \mu\text{m}$) to old melting snow ($r = 1000 \mu\text{m}$) can reduce broadband albedo by $\sim 10\%$. By comparison, adding 20 ng g^{-1} of BC, which has been found in the top layer of melting GrIS snow, reduces albedo by only 1–2%.

The difference between MAR and GLASS trends cannot be driven solely by the MODIS sensor degradation on the TERRA satellite (used in the GLASS product), because the estimated impact of sensor degradation on the albedo trend is much smaller than the difference between the MAR and GLASS trends, and because the GLASS product was obtained by combining data from both TERRA and AQUA satellites, hence likely reducing the impact of the TERRA sensor degradation on the trends. Instead, since MAR does not account for the presence of surface impurities, and because the impact of impurities is mostly in the UV and visible portion of the spectrum, we suggest that the difference of $-0.017 \text{ decade}^{-1}$ between the MAR and GLASS visible albedo trends can be attributed to increasing mixing ratios of impurities in surface snow on some parts of the GrIS. As we pointed out, this could be due to a combination of increased exposure of dirty ice with ablation (Wientjes and Oerlemans, 2010; Bøggild et al., 2010), to enhanced melt consolidation with warming (e.g., Doherty et al., 2013), or to increased deposition of impurities from the atmosphere. The absence of in situ, spatially distributed measurements to separate these processes means that we cannot quantify their relative contributions to the darkening in the visible region. Based on our analysis of trends in AOD over Greenland and the lack of a trend in forest-fire counts in North America and Eurasia, we argue that increased deposition of light-absorbing impurities is not a large driver for the observed negative trends in Greenland surface albedo. An exception could be an increase in the deposition of locally-transported dust near the glacial margins, which would primarily

The darkening of the Greenland ice sheet

M. Tedesco et al.

Title Page

Abstract

Introduction

Conclusions

References

Tables

Figures



Back

Close

Full Screen / Esc

Printer-friendly Version

Interactive Discussion



affect the ablation zone. In particular, locally lofted dust may be playing a substantial role in the southwest GrIS ablation zone. However, we note that increased deposition is not needed in order to have an increase in the concentration of impurities at the GrIS surface. As noted above, indeed, temperatures and melt rates have been accelerating over the GrIS during the past decades (e.g., Tedesco et al., 2014). When snow melts, snow water is removed from the surface more efficiently than particulate impurities; the result is an increase in impurity concentrations in surface snow (e.g. Flanner et al., 2007; Doherty et al., 2013). Large particles, such as dust, in particular, will have poor mobility through the snowpack (Conway et al., 1996) so their concentration at the surface is expected to increase with snowmelt. This effect may be especially amplifying snow impurity content in the low-altitude ablation zone of the GrIS, where enhanced melting has been occurring (e.g., Tedesco et al., 2014). Further, the albedo reduction for a given concentration of an absorbing impurity in snow is greater in large-grained snow than in small-grained snow (Fig. 7 of Warren and Wiscombe, 1980; Flanner et al., 2007), so climate warming itself will amplify the effect of impurities on surface albedo. Warming may also lead to increased sublimation, removing snow water but not particles from the snow surface, again increasing concentrations of impurities in surface snow.

The presence of surface impurities also promotes the evolution of the so-called “bioalbedo”, with biological growth on the surface depressing the albedo. Green, pink, purple, brown and black pigmented algae, indeed, occur in melting snow and ice. Microbes can bind to particulates, including BC, retaining them at the surface in higher concentrations than in the parent snow and ice. The magnitude of this source of darkening is currently unquantified, but as the climate warms and melt seasons lengthen, biological habitats are expected to expand, with their contribution to darkening likely increasing (Benning et al., 2014).

Quantifying the impact of aerosols on Greenland darkening is also made difficult by the large disagreements among models in their predicted aerosol deposition rates over the GrIS. For example, in Fig. 11 we examine the contrast between AOD trends

The darkening of the Greenland ice sheet

M. Tedesco et al.

Title Page

Abstract

Introduction

Conclusions

References

Tables

Figures



Back

Close

Full Screen / Esc

Printer-friendly Version

Interactive Discussion



from the MACC model used by Dumont et al. (2014) and the Goddard Chemistry Aerosol Radiation and Transport model (GOCART). The GOCART model simulates major tropospheric aerosol components, including sulphate, dust, BC, organic carbon (OC), and sea-salt aerosols using assimilated meteorological fields of the Goddard Earth Observing System Data Assimilation System (GEOS DAS), generated by the Goddard Global Modeling and Assimilation Office. Figure 11 compares results for AOD at 550 nm from MACC and GOCART for dust, organic matter and black carbon for the domain bounded by 75–80° N and 30–50° W (the same area considered by Dumont et al., 2014). The MACC model shows no significant trend in deposited aerosols, and MACC shows a trend only for dust (Fig. 11).

Neither model captures trends in exposed silt/dust as Greenland glaciers have receded, and therefore we would not expect them to capture trends in dust from this source. The inconsistency between MACC and GOCART values and trends is puzzling, and indicates that simulation of absolute aerosol deposition rates over Greenland needs improvement.

Light-absorbing impurities in snow affect albedo not only directly, but also indirectly by absorbing sunlight, warming the snowpack, and accelerating snow grain size growth. We started studying the magnitude of this “indirect effect” of impurities on snow grain size, and therefore albedo, by modifying the albedo scheme within MAR. Specifically, we reduced the visible component of the albedo, α_1 in Eq. (2), by between 0.01 and 0.05 to simulate the effects of impurities. This was, in turn, used in Eq. (1) to compute the broadband albedo. The value of 0.05 was estimated as the maximum estimated albedo decrease for BC concentrations measured in the cold snow and percolation zones of the GIS. The value of –0.05 used in our simulations for each iteration of MAR likely overestimates the effect of impurities on grain size at the beginning of the melting season, but underestimates the effect during the melting season when impurities tend to concentrate at the snow surface (Doherty et al., 2013). Higher concentrations of impurities are present along the margins of the ice sheet because of their proximity to local sources of dust and the proliferation of algae and microorganisms on the ice

The darkening of the Greenland ice sheet

M. Tedesco et al.

Title Page

Abstract

Introduction

Conclusions

References

Tables

Figures



Back

Close

Full Screen / Esc

Printer-friendly Version

Interactive Discussion



surface, so the effect of impurities on grain size is likely larger there. Still the results of this synthetic experiment can provide an initial indication of the indirect effect of impurities on the evolution of the snowpack and its albedo. We specifically focused for our experiment on an area of $100 \times 100 \text{ km}^2$ centred at Swiss Camp, one of the Greenland Climate Network stations (Steffen and Box, 2001) for the summer of 2012. Figure 12 shows daily broadband albedo simulated by MAR, with and without the imposed albedo reductions of 0.01, 0.03 and 0.05 in the visible albedo. The differences in broadband albedo between the default case (pure snow) and the cases simulating dirty snow are relatively constant and equal to the imposed albedo reduction, until the end of May, when substantial melting begins (e.g., Tedesco et al., 2013). After this, all cases show broadband albedo lowered by an amount as low as the imposed visible albedo reduction. The presence of new snowfall during the first week of June increases albedo temporarily, with the “dirty snow” case (albedo reduction of 0.05) showing the fastest return to reduced albedo after the new snowfall. This can be explained by the accelerated grain growth induced by the increased absorbed solar radiation (Fig. 12b), which is due to the reduced albedo in the visible region (i.e. the presence of absorbing impurities). A similar behaviour is simulated for the precipitation events occurring during the second week of August, though in this case the minimum albedo values obtained in the different cases are dependent on the introduced negative albedo anomaly (i.e. snow impurity content). This is in contrast to the behaviour during the snowfall event in the month of July when there is persistent melting; here, all cases show similar albedo values. We performed a linear regression between the grain sizes simulated for clean snow and for snow with the three imposed reductions in visible-band simulating the presence of light-absorbing impurities. These regressions had slopes of 1.0099 ($R^2 = 0.92$, -0.01 bias), 1.0037 ($R^2 = 0.91$, -0.03 bias) and 1.0094 ($R^2 = 0.9$, -0.05 bias) when considering all grain sizes. The slope between grain sizes in dirty vs. clean snow increase to 1.0529 ($R^2 = 0.89$, -0.01 bias), 1.0656 ($R^2 = 0.9$, -0.03 bias) and 1.0676 ($R^2 = 0.89$, -0.05 bias) when considering only cases where grain size is less than 0.6 mm. This value was selected based on an analysis of the temporal

evolution of grain size (Fig. 12b) as characterising the presence of persistent melting. The percentage difference between simulated grain sizes in clean pure vs. dirty snow (Table 3) indicates that grain sizes are typically only about 1 % larger for dirty snow typical of the GIS dry snow and percolation zones, though these differences can be as high as 15–20 % during the period of snow metamorphosis and melting following new snowfall.

6 Summary and conclusions

We studied the mean summer broadband albedo over the Greenland ice sheet between 1981 and 2012 as estimated from spaceborne measurements and found that summer albedo decreased at a rate of 0.02 decade^{-1} between 1996 and 2012. The analysis of the outputs of the MAR regional climate model indicates that the observed darkening can be associated with increasing temperatures and enhanced melting occurring during the same period, and promoting increased surface snow grain size as well as the expansion and persistency of areas with exposed bare ice. Although the MAR model can simulate the interannual variability of GLASS albedo, the larger magnitude of the trends in the GLASS albedo with respect to those obtained with MAR indicates that other processes beside those represented in the MAR physics need to be accounted for. We identified such processes in the increased surface impurity concentration associated with the appearance of dirty ice and consolidation with snowmelt. The analysis of modelled and in situ datasets indicated an absence of trends in aerosol optical depth over Greenland. This is consistent with the absence of trends in surface aerosol concentrations measured around the Arctic. Consequently, we suggest that the increased surface concentrations of impurities associated with the darkening is not related to increased deposition of impurities, but rather to post-depositional processes, including increased loss of snow water to sublimation and melt and the outcropping of “dirty” underlying ice associated with snow/firn removal due to ablation. Future projections of GrlS albedo obtained from MAR forced under different

The darkening of the Greenland ice sheet

M. Tedesco et al.

Title Page

Abstract

Introduction

Conclusions

References

Tables

Figures



Back

Close

Full Screen / Esc

Printer-friendly Version

Interactive Discussion



warming scenarios point to continued darkening through the end of the century, with regions along the edges of the ice sheet subject to the largest decrease, driven solely by warming-driven changes in snow grain size, exposure of bare ice, and melt pool formation. We hypothesise that projected darkening trends would be even greater in view of the underestimated projected melting (and effect on albedo) and in view of the fact that the current version of the MAR model does not account for the presence of surface impurities and the associated positive direct and indirect impact on lowered albedo.

The drivers we identified to be responsible for the observed darkening are related to endogenous processes rather than exogenous ones and are strongly driven by melting. Because melting is projected to increase over the next decades, it is crucial to assess the state of the art of studying, quantifying and projecting these processes as they will inevitably impact, and be impacted by, future scenarios. Intrinsic limitations of current observational tools and techniques, the scarcity of in situ observations, and the albedo schemes currently used in existing models of surface energy balance and mass balance limit our ability to separate the contributions to darkening by the different processes, especially with regard to the cause and evolution of surface impurity concentrations. Moreover, as with all instruments, sensors undergo deterioration, and it can be difficult to separate an albedo trend from sensor drift. This is especially true in the dry-snow zone, where impurity concentrations are extremely low (only a few ppb in the case of BC).

Remote sensing and in situ observations should be complemented with models that simulate the surface energy balance to account for the evolution of the snowpack, in particular changes in surface grain size and exposure of bare ice. Simulations with regional climate models can provide such quantities, but they do not currently account for the transport and deposition of impurities to Greenland, the post-depositional evolution of impurities in the snowpack, and the synergism between surface impurities and grain growth (whereby a given impurity content causes more albedo reduction in coarse-grained snow than in fine-grained snow). In this regard, the

The darkening of the Greenland ice sheet

M. Tedesco et al.

Title Page

Abstract

Introduction

Conclusions

References

Tables

Figures



Back

Close

Full Screen / Esc

Printer-friendly Version

Interactive Discussion



current parameterisation for snow albedo in MAR is based on that of Brun et al. (1992), as part of an avalanche-forecasting model. As a consequence of the results of this study, we began evaluating an alternative albedo scheme using a parameterisation that can also account for the albedo reduction by absorptive impurities (e.g. Dang et al., 2015). Moreover, we are also considering using the firn/ice albedo parameterisation of Dadic et al. (2013), based on measurements covering the range of densities from 400 to 900 kg m⁻³.

Surface-based measurements are needed to test satellite-retrieved albedo and to quantify the drivers behind albedo changes in different areas of Greenland. To date, most surface-based observations have been made in the dry-snow zone or the percolation zone, and they have generally focused on measuring the mixing ratios of BC (Hagler et al. 2007; McConnell et al. 2007) or of the spectral light absorption by all particulate components collectively (Doherty et al., 2010; Hegg et al., 2009, 2010). The regions of Greenland that are darkening the most rapidly are within the ablation zone. Here, there is no direct evidence that the rate of atmospheric deposition of impurities has been increasing. Still, in view of the cumulative effect of snowmelt leaving impurities at the surface, the intra-seasonal variation of deposition may not be as important as the exposure of impurities by melting. Changes in the abundances of light-absorbing algae and other organic material with warmer temperatures may also be contributing to declining albedo, particularly for the ice, but this is an essentially un-studied source of darkening. Until measurements are made that quantify and distinguish the relative roles of each of these factors in the darkening of the GrIS, it is not possible to reduce the uncertainty on estimating their contributions to the acceleration of surface melt. In addition to the need for targeted ground observations, it is necessary for the models that simulate and project the evolution of surface conditions over Greenland to start including the contribution of surface impurities, their processes, and their impact on albedo, as well as aerosol models that account for their deposition. Concurrently, spaceborne sensors or missions capable of separating the contributions from the

different processes (with increased spatial, spectral and radiometric resolution) should be planned for remote sensing to become a more valuable tool in this regard.

Author contributions. M. Tedesco conceived the study, carried out the scientific analysis and wrote the main body of the manuscript. S. Doherty co-wrote the manuscript and provided feedback on the analysis of the impact of surface impurities on the albedo decrease. E. Noble provided the MAR simulations for the sensitivity of grain-size evolution to changes in the visible albedo. P. Alexander provided MODIS visible data for the comparison with the GLASS-estimated visible albedo. J. Jeyaratnam supported the reprojection and analysis of GLASS and MAR data. X. Fettweis contributed with the analysis of MAR outputs. M. Tedesco, S. Doherty, X. Fettweis and J. Stroeve edited the final version of the manuscript.

Acknowledgements. M. Tedesco and P. Alexander were supported by NSF grants PLR1304807 and ANS 0909388, and NASA grant NNX1498G. The authors are grateful to Kostas Tsirigadis (NASA GISS) for providing the outputs of GISS modelE of the AeroCom phase II project and to Marie Dumont, Eric Brun and Samuel Morin for the data used in Fig. 11.

We thank Tao He at the University of Maryland, College Park, for the discussion on the GLASS product. The authors thank Stephen Warren for providing suggestions and guidance during the preparation of the manuscript, particularly for pointing out limitations and providing suggestions on the albedo parameterisations.

References

- Alexander, P. M., Tedesco, M., Fettweis, X., van de Wal, R. S. W., Smeets, C. J. P. P., and van den Broeke, M. R.: Assessing spatio-temporal variability and trends in modelled and measured Greenland Ice Sheet albedo (2000–2013), *The Cryosphere*, 8, 2293–2312, doi:10.5194/tc-8-2293-2014, 2014.
- Arnaud, L., Barnola, J. M., and Duval, P.: Physical modeling of the densification of snow/firn and ice in the upper part of polar ice sheets, in: *Physics of Ice Core Records*, edited by: Hondoh, T., Hokkaido University Press, Sapporo, Japan, 285–305, 2000.
- Arora, V. K. and Boer, G. J.: Uncertainties in the 20th century carbon budget associated with land use change, *Glob. Change Biol.*, 16, 3327–3348, doi:10.1111/j.1365-2486.2010.02202.x, 2010.

TCO

9, 5595–5645, 2015

The darkening of the Greenland ice sheet

M. Tedesco et al.

Title Page

Abstract

Introduction

Conclusions

References

Tables

Figures



Back

Close

Full Screen / Esc

Printer-friendly Version

Interactive Discussion



The darkening of the Greenland ice sheet

M. Tedesco et al.

Title Page

Abstract

Introduction

Conclusions

References

Tables

Figures



Back

Close

Full Screen / Esc

Printer-friendly Version

Interactive Discussion



- Benning, L. G., Anesio, A. M., Lutz, S., and Tranter, M.: Biological impact on Greenland's albedo, *Nat. Geosci.*, 7, 691, doi:10.1038/ngeo2260, 2014.
- Benson, C. S.: Stratigraphic Studies in the Snow and Firn of the Greenland Ice Sheet, Research Report 70, U.S. Army Snow, Ice, and Permafrost Research Establishment (SIPRE), 93 pp., 1962.
- Bøggild, C. E., Brandt, R. E., Brown, K. J., and Warren, S. G.: The ablation zone in northeast Greenland: ice types, albedos, and impurities, *J. Glaciol.*, 56, 101–113, 2010.
- Bond, T. C., Doherty, S. J., Fahey, D. W., Forster, P. M., Berntsen, T., DeAngelo, B. J., Flanner, M. G., Ghan, S., Kärcher, B., Koch, D., Kinne, S., Kondo, Y., Quinn, P. K., Sarofim, M. C., Schultz, M. G., Schulz, M., Venkataraman, C., Zhang, H., Zhang, S., Bellouin, N., Guttikunda, S. K., Hopke, P. K., Jacobon, M. Z., Kaiser, J. W., Klimont, Z., Lohmann, U., Schwarz, J. P., Shindell, D., Storelvmo, T., Warren, S. G. and Zender, C. S.: Bounding the role of black carbon in climate: a scientific assessment, *J. Geophys. Res.*, 118, 5380–5552, doi:10.1002/jgrd.50171, 2013.
- Box, J. E., Fettweis, X., Stroeve, J. C., Tedesco, M., Hall, D. K., and Steffen, K.: Greenland ice sheet albedo feedback: thermodynamics and atmospheric drivers, *The Cryosphere*, 6, 821–839, doi:10.5194/tc-6-821-2012, 2012.
- Brun, E., David, P., Sudul, M., and Brunot, G.: A numerical model to simulate snow-cover stratigraphy for operational avalanche forecasting, *J. Glaciol.*, 38, 13–22, 1992.
- Cachier, H. and Pertuisot, M. H.: Particulate carbon in Arctic ice, *Analisis*, 22, 34–37, 1994.
- Ch'ylek, P., Johnson, B., Damiano, P. A., Taylor, K. C., and Clement, P.: Biomass burning record and black carbon in the GISP2 ice core, *Geophys. Res. Lett.*, 22, 89–92, 1995.
- Chylek, P., Li, J., Dubey, M. K., Wang, M., and Lesins, G.: Observed and model simulated 20th century Arctic temperature variability: Canadian Earth System Model CanESM2, *Atmos. Chem. Phys. Discuss.*, 11, 22893–22907, doi:10.5194/acpd-11-22893-2011, 2011.
- Clarke, A. D. and Noone, K. J.: Soot in the Arctic snowpack: A cause for perturbations in radiative transfer, *Atmos. Environ.*, 19, 2045–2053, 1985.
- Conway, H., Gades, A., and Raymond, C. F.: Albedo of dirty snow during conditions of melt, *Water Resour. Res.*, 32, 1713–1718, 1996.
- Dadic, R., Mullen, P. C., Schneebeli, M., Brandt, R. E., and Warren, S. G.: Effects of bubbles, cracks, and volcanic tephra on the spectral albedo of bare ice near the Trans-Antarctic Mountains: implications for sea-glaciers on Snowball Earth, *J. Geophys. Res.-Earth*, 118, 1658–1676, doi:10.1002/jgrf.20098, 2013.

The darkening of the Greenland ice sheet

M. Tedesco et al.

Title Page

Abstract

Introduction

Conclusions

References

Tables

Figures

◀

▶

◀

▶

Back

Close

Full Screen / Esc

Printer-friendly Version

Interactive Discussion



Dang, C., Brandt, R. E., and Warren, S. G.: Parameterizations for narrowband and broadband albedo of pure snow, and snow containing mineral dust and black carbon, *J. Geophys. Res.-Atmos.*, 120, 5446–5468, doi:10.1002/2014JD022646, 2015.

De Ridder, K. and Galle' H: Land surface-induced regional climate change in Southern Israel, *Appl. Meteorol.*, 37, 1470–1485, 1998.

Doherty, S. J., Warren, S. G., Grenfell, T. C., Clarke, A. D., and Brandt, R. E.: Light-absorbing impurities in Arctic snow, *Atmos. Chem. Phys.*, 10, 11647–11680, doi:10.5194/acp-10-11647-2010, 2010.

Doherty, S. J., Grenfell, T. C., Forsström, S., Hegg, D. L., Brandt, R. E., and Warren, S. G.: Observed vertical redistribution of black carbon and other insoluble light-absorbing particles in melting snow, *J. Geophys. Res.-Atmos.* 118, 5553–5569, 2013.

Dumont, M., Brun, E., Picard, G., Michou, M., Libois, Q., Petit, J.-R., Geyer, M., Morin, S., and Josse, B.: Contribution of light-absorbing impurities in snow to Greenland's darkening since 2009, *Nat. Geosci.*, 7, 509–512, 2014.

Fettweis, X., Gallée, H., Lefebvre, F., and van Ypersele, J.-P.: Greenland surface mass balance simulated by a regional climate model and comparison with satellite-derived data in 1990–1991, *Clim. Dynam.*, 24, 623–640, 2005.

Fettweis, X., Franco, B., Tedesco, M., van Angelen, J. H., Lenaerts, J. T. M., van den Broeke, M. R., and Gallée, H.: Estimating the Greenland ice sheet surface mass balance contribution to future sea level rise using the regional atmospheric climate model MAR, *The Cryosphere*, 7, 469–489, doi:10.5194/tc-7-469-2013, 2013.

Flanner, M. G., Zender, C. S., Randerson, J. T., and Rasch, P. J.: Present-day climate forcing and response from black carbon in snow, *J. Geophys. Res.*, 112, D11202, doi:10.1029/2006JD008003, 2007.

Grenfell, T. C., Perovich, D. K., and Ogren, J. A.: Spectral albedos of an alpine snowpack, *Cold Reg. Sci. Technol.*, 4, 121–127, 1981.

Greuell, W. and Konzelman, T.: Numerical modelling of the energy balance and the englacial temperature of the Greenland Ice Sheet, calculations for the ETH-Camp location (West Greenland, 1155 m a.s.l.), *Global Planet. Change*, 9, 91–114, 1994.

Hagler, G. S. W., Bergin, M. H., Smith, E. A., and Dibb, J. E.: A summer time series of particulate carbon in the air and snow at Summit, Greenland, *J. Geophys. Res.*, 112, D21309, doi:10.1029/2007JD008993, 2007.

**The darkening of the
Greenland ice sheet**

M. Tedesco et al.

[Title Page](#)[Abstract](#)[Introduction](#)[Conclusions](#)[References](#)[Tables](#)[Figures](#)[I◀](#)[▶I](#)[◀](#)[▶](#)[Back](#)[Close](#)[Full Screen / Esc](#)[Printer-friendly Version](#)[Interactive Discussion](#)

- He, T., Liang, S., Yu, Y., Wang, D., Gao, F., and Liu, Q.: Greenland surface albedo changes in July 1981–2012 from satellite observations, *Environ. Res. Lett.*, 8, 044043, doi:10.1088/1748-9326/8/4/044043, 2013.
- 5 Hegg, D. A., Warren, S. G., Grenfell, T. C., Doherty, S. J., Larson, T. V., and Clarke, A. D.: Source attribution of black carbon in Arctic snow, *Environ. Sci. Technol.*, 43, 4016–4021, 2009.
- Hegg, D. A., Warren, S. G., Grenfell, T. C., Doherty, S. J., and Clarke, A. D.: Sources of light-absorbing aerosol in arctic snow and their seasonal variation, *Atmos. Chem. Phys.*, 10, 10923–10938, doi:10.5194/acp-10-10923-2010, 2010.
- 10 Herron, M. M. and Langway, Jr., C. C.: Firn densification: an empirical model, *J. Glaciol.*, 25, 373–385, 1980.
- Ichoku, C. and Ellison, L.: Global top-down smoke-aerosol emissions estimation using satellite fire radiative power measurements, *Atmos. Chem. Phys.*, 14, 6643–6667, doi:10.5194/acp-14-6643-2014, 2014.
- 15 Keegan, K. M., Albert, M. R., McConnell, J. R., and Baker, I.: Climate change and forest fires synergistically drive widespread met events of the Greenland Ice Sheet, *P. Natl. Acad. Sci. USA*, 111, 7964–7967, doi:10.1073/pnas.1405397111, 2014.
- LaChapelle, E. R.: *Field Guide to Snow Crystals*, University of Washington Press, Seattle, 1969.
- 20 Jiao, C., Flanner, M. G., Balkanski, Y., Bauer, S. E., Bellouin, N., Berntsen, T. K., Bian, H., Carslaw, K. S., Chin, M., De Luca, N., Diehl, T., Ghan, S. J., Iversen, T., Kirkevåg, A., Koch, D., Liu, X., Mann, G. W., Penner, J. E., Pitari, G., Schulz, M., Seland, Ø., Skeie, R. B., Steenrod, S. D., Stier, P., Takemura, T., Tsigaridis, K., van Noije, T., Yun, Y., and Zhang, K.: An AeroCom assessment of black carbon in Arctic snow and sea ice, *Atmos. Chem. Phys.*, 14, 2399–2417, doi:10.5194/acp-14-2399-2014, 2014.
- 25 Lefebre, F., Gallée, H., and van Ypersele, J.-P.: Modeling of snow and ice melt at ETH Camp (West Greenland): a study of surface albedo, 108, 4231, doi:10.1029/2001JD001160, 2003.
- Liang, S., Zhao, X., Liu, S., Yuan, W., Cheng, X., Xiao, Z., Zhang, X., Liu, Q., Cheng, J., Tang, H., Qu, Y., Bo, Y., Y., Qu, Ren, H., Yu, K., and Townshend, J.: A long-term Global Land Surface Satellite (GLASS) data-set for environmental studies, *International Journal of Digital Earth*, 6, 5–33, 2013.
- 30 Loeb, N.: In-flight calibration of NOAA AVHRR visible and near-IR bands over Greenland and Antarctica, *Int. J. Remote Sens.*, 18, 477–490, 1997.

The darkening of the Greenland ice sheet

M. Tedesco et al.

Title Page

Abstract

Introduction

Conclusions

References

Tables

Figures

◀

▶

◀

▶

Back

Close

Full Screen / Esc

Printer-friendly Version

Interactive Discussion



- Masonis, S. J. and Warren, S. G.: Gain of the AVHRR visible channel as tracked using bidirectional reflectance of Antarctic and Greenland snow, *Int. J. Remote Sens.*, 22, 1495–1520, 2001.
- 5 McConnell, J. R., Edwards, R., Kok, G. L., Flanner, M. G., Zender, C. S., Saltzman, E. S., Banta, J. R., Pasteris, D. R., Carter, M. M., and Kahl, J. D. W.: 20th century industrial black carbon emissions altered Arctic climate forcing, *Science*, 317, 1381–1384, doi:10.1126/science.1144856, 2007.
- 10 Meinshausen, M., Smith, S. J., Calvin, K., Daniel, J. S., Kainuma, M. L. T., Lamarque, J.-F., Matsumoto, K., Montzka, S. A., Raper, S. C. B., Riahi, K., Thomson, A., Velders, G. J. M., and van Vuuren, D. P. P.: The RCP greenhouse gas concentrations and their extensions from 1765 to 2300, *Climatic Change*, 109, 213–241, 2011.
- Moss, R. H., Edmonds, J. A., Hibbard, K. A., Manning, M. R., Rose, S. K., van Vuuren, D. P., Carter, T. R., Emori, S., Kainuma, M., Kram, T., Meehl, G. A., Mitchell, J. F. B., Nakicenovic, N., Riahi, K., Smith, S. J., Stouffer, R. J., Thomson, A. M., Weyant, J. P., and Wilbanks, T. J.: The next generation of scenarios for climate change research and assessment, *Nature*, 463, 747–756, 2010.
- 15 Myhre, G., Samset, B. H., Schulz, M., Balkanski, Y., Bauer, S., Bernsten, T. K., Bian, H., Bellouin, N., Chin, M., Diehl, T., Easter, R. C., Feichter, J., Ghan, S. J., Hauglustaine, D., Iversen, T., Kinne, S., Kirkevåg, A., Lamarque, J.-F., Lin, G., Liu, X., Lund, M. T., Luo, G., Ma, X., van Noije, T., Penner, J. E., Rasch, P. J., Ruiz, A., Seland, Ø., Skeie, R. B., Stier, P., Takemura, T., Tsigaridis, K., Wang, P., Wang, Z., Xu, L., Yu, H., Yu, F., Yoon, J.-H., Zhang, K., Zhang, H., and Zhou, C.: Radiative forcing of the direct aerosol effect from AeroCom Phase II simulations, *Atmos. Chem. Phys.*, 13, 1853–1877, doi:10.5194/acp-13-1853-2013, 2013.
- 20 Nghiem, S. V., Hall, D. K., Mote, T. L., Tedesco, M., Albert, M. R., Keegan, K., Shuman, C. A., DiGirolamo, N. E., and Neumann, G.: The extreme melt across the Greenland ice sheet in 2012, *Geophys. Res. Lett.*, 39, L20502, doi:10.1029/2012GL053611, 2012.
- 25 Rae, J. G. L., Aðalgeirsdóttir, G., Edwards, T. L., Fettweis, X., Gregory, J. M., Hewitt, H. T., Lowe, J. A., Lucas-Picher, P., Mottram, R. H., Payne, A. J., Ridley, J. K., Shannon, S. R., van de Berg, W. J., van de Wal, R. S. W., and van den Broeke, M. R.: Greenland ice sheet surface mass balance: evaluating simulations and making projections with regional climate models, *The Cryosphere*, 6, 1275–1294, doi:10.5194/tc-6-1275-2012, 2012.
- 30

The darkening of the Greenland ice sheet

M. Tedesco et al.

Title Page

Abstract

Introduction

Conclusions

References

Tables

Figures

◀

▶

◀

▶

Back

Close

Full Screen / Esc

Printer-friendly Version

Interactive Discussion



- Rignot, E., Velicogna, I., van den Broeke, M. R., Monaghan, A., and Lenaerts, J. T. M.: Acceleration of the contribution of the Greenland and Antarctic ice sheets to sea level rise, *Geophys. Res. Lett.*, 38, L05503, doi:10.1029/2011GL046583, 2011.
- 5 Samset, B. H., Myhre, G., Herber, A., Kondo, Y., Li, S.-M., Moteki, N., Koike, M., Oshima, N., Schwarz, J. P., Balkanski, Y., Bauer, S. E., Bellouin, N., Bernsten, T. K., Bian, H., Chin, M., Diehl, T., Easter, R. C., Ghan, S. J., Iversen, T., Kirkevåg, A., Lamarque, J.-F., Lin, G., Liu, X., Penner, J. E., Schulz, M., Seland, Ø, Skeie, R. B., Stier, P., Takemura, T., Tsigaridis, K., and Zhang, K.: Modeled black carbon radiative forcing and atmospheric lifetime in AeroCom Phase II constrained by aircraft observations, *Atmos. Chem. Phys. Discuss.*, 14, 20083–20115, doi:10.5194/acpd-14-20083-2014, 2014.
- 10 Schaaf, C. B., Gao, F., Strahler, A. H., Lucht, W., Li, X., Tsang, T., Strugnell, N. C., Zhang, X., Jin, Y., Muller, J. P., Lewis, P., Barnsley, M., Hobson, P., Disney, M., Roberts, G., Dunderdale, M., Doll, C., d'Entremont, R. P., Hu, B., Liang, S., Privette, J. L., and Roy, D.: First operational BRDF, albedo nadir reflectance products from MODIS, *Remote Sens. Environ.*, 115, 1296–1300, 2002.
- 15 Seland, O., Iversen, T., Kirkevåg, A., and Storelvmo, T.: Aerosol-climate interactions in the CAM-Oslo atmospheric GCM and investigation of associated basic shortcomings, *Tellus A*, 60, 459–491, doi:10.1111/j.1600-0870.2008.00318.x, 2008.
- Shepherd, A., Ivins, E., Geruo, A., et al.: A reconciled estimate of ice-sheet mass balance, *Science*, 338, 1183–1189, 2012.
- 20 Steffen, K. and Box, J. E.: Surface climatology of the Greenland ice sheet: Greenland Climate Network 1995–1999, *J. Geophys. Res.*, 106, 33951–33964, 2001.
- Stohl, A., Andrews, E., Burkhardt, J. F., Forster, C., Herber, A., Hoch, S. W., Kowal, D., Lunder, C., Mefford, T., Orgren, J. A., Sharma, S., Spichtinger, N., Stebel, K., Stone, R., Ström, J., Tørseth, K., Wehrli, C., and Yttri, K. E.: Pan-Arctic enhancement of light absorbing aerosol concentration due to North American boreal forest fires during summer 2004, *J. Geophys. Res.*, 111, D22214, doi:10.1029/2006JD007216, 2006.
- 25 Stone, R. S., Sharma, S., Herber, A., Eleftheriadis, K., and Nelson, D. W.: A characterization of Arctic aerosols on the basis of aerosol optical depth and black carbon measurements, *Elementa: Science of the Anthropocene*, 2, 000027, doi:10.12952/journal.elementa.000027, 2014.
- 30

The darkening of the Greenland ice sheet

M. Tedesco et al.

Title Page

Abstract

Introduction

Conclusions

References

Tables

Figures



Back

Close

Full Screen / Esc

Printer-friendly Version

Interactive Discussion



Stroeve, J., Box, J. E., Gao, F., Liang, S., Nolin, A., and Schaaf, C.: Accuracy assessment of the MODIS 16-day albedo product for snow: comparisons with Greenland in situ measurements, *Remote Sens. Environ.*, 94, 46–60, 2005.

Stroeve, J., Box, J. E., Wang, Z., Schaaf, C., and Barrett, A.: Re-evaluation of MODIS MCD43 Greenland albedo accuracy and trends, *Remote Sens. Environ.*, 138, 199–214, 2013.

Tedesco, M. and Fettweis, X.: 21st century projections of surface mass balance changes for major drainage systems of the Greenland ice sheet, *Environ. Res. Lett.*, 7, 045405, doi:10.1088/1748-9326/7/4/045405, 2012.

Tedesco, M., Fettweis, X., Broeke, M. R. V. D., de Wal, R. S. W. V., Smeets, C. J. P. P., de Berg, W. J. V., Serreze, M. C., and Box, J. E.: The role of albedo and accumulation in the 2010 melting record in Greenland, *Environ. Res. Lett.*, 6, 014005, doi:10.1088/1748-9326/6/1/014005, 2011.

Tedesco, M., Fettweis, X., Mote, T., Wahr, J., Alexander, P., Box, J. E., and Wouters, B.: Evidence and analysis of 2012 Greenland records from spaceborne observations, a regional climate model and reanalysis data, *The Cryosphere*, 7, 615–630, doi:10.5194/tc-7-615-2013, 2013.

Tedesco, M., Box, J. E., Cappelen, J., Fettweis, X., Mote, T., Rennermalm, A. K., van de Wal, R. S. W., and Wahr, J.: Greenland Ice Sheet in [2013 NOAA Arctic Report Card], 2014.

Tedesco, M., Doherty, S., Warren, W., Tranter, M., Stroeve, J., Fettweis, X., and Alexander, P.: What darkens the Greenland Ice Sheet?, *Eos*, 96, doi:10.1029/2015EO035773, 2015.

Tsigaridis, K., Daskalakis, N., Kanakidou, M., Adams, P. J., Artaxo, P., Bahadur, R., Balkanski, Y., Bauer, S. E., Bellouin, N., Benedetti, A., Bergman, T., Berntsen, T. K., Beukes, J. P., Bian, H., Carslaw, K. S., Chin, M., Curci, G., Diehl, T., Easter, R. C., Ghan, S. J., Gong, S. L., Hodzic, A., Hoyle, C. R., Iversen, T., Jathar, S., Jimenez, J. L., Kaiser, J. W., Kirkevåg, A., Koch, D., Kokkola, H., Lee, Y. H., Lin, G., Liu, X., Luo, G., Ma, X., Mann, G. W., Mihalopoulos, N., Morcrette, J.-J., Müller, J.-F., Myhre, G., Myriokefalitakis, S., Ng, S., O'Donnell, D., Penner, J. E., Pozzoli, L., Pringle, K. J., Russell, L. M., Schulz, M., Sciare, J., Seland, Ø., Shindell, D. T., Sillman, S., Skeie, R. B., Spracklen, D., Stavrou, T., Steenrod, S. D., Takemura, T., Tiitta, P., Tilmes, S., Tost, H., van Noije, T., van Zyl, P. G., von Salzen, K., Yu, F., Wang, Z., Wang, Z., Zaveri, R. A., Zhang, H., Zhang, K., Zhang, Q., and Zhang, X.: The AeroCom evaluation and intercomparison of organic aerosol in global models, *Atmos. Chem. Phys. Discuss.*, 14, 6027–6161, doi:10.5194/acpd-14-6027-2014, 2014.

The darkening of the Greenland ice sheet

M. Tedesco et al.

Title Page

Abstract

Introduction

Conclusions

References

Tables

Figures



Back

Close

Full Screen / Esc

Printer-friendly Version

Interactive Discussion



- van Angelen, J. H., Lenaerts, J. T. M., Lhermitte, S., Fettweis, X., Kuipers Munneke, P., van den Broeke, M. R., van Meijgaard, E., and Smeets, C. J. P. P.: Sensitivity of Greenland Ice Sheet surface mass balance to surface albedo parameterization: a study with a regional climate model, *The Cryosphere*, 6, 1175–1186, doi:10.5194/tc-6-1175-2012, 2012.
- 5 van den Broeke, M. R., Smeets, C. J. P. P., and van de Wal, R. S. W.: The seasonal cycle and interannual variability of surface energy balance and melt in the ablation zone of the west Greenland ice sheet, *The Cryosphere*, 5, 377–390, doi:10.5194/tc-5-377-2011, 2011.
- Vernon, C. L., Bamber, J. L., Box, J. E., van den Broeke, M. R., Fettweis, X., Hanna, E., and Huybrechts, P.: Surface mass balance model intercomparison for the Greenland ice sheet, *The Cryosphere*, 7, 599–614, doi:10.5194/tc-7-599-2013, 2013.
- 10 Wang, D., Morton, D., Masek, J., Wu, A., Nagol, J., Xiong, X., Levy, R., Vermote, E., and Wolfe, R.: Impact of sensor degradation on the MODIS NDVI time series, *Remote Sens. Environ.*, 119, 55–61, 2012.
- Warren, S. G.: Optical properties of snow, *Rev. Geophys. Space Ge.*, 20, 67–89, 1982.
- 15 Warren, S. G.: Can black carbon in snow be detected by remote sensing?, *J. Geophys. Res.-Atmos.*, 118, 779–786, 2013.
- Warren, S. G. and Wiscombe, W. J.: A model for the spectral albedo of snow – Part 2: Snow containing atmospheric aerosols, *J. Atmos. Sci.*, 37, 2734–2745, 1980.
- Watanabe, M., Suzuki, T., O’ishi, R., Komuro, Y., Watanabe, S., Emori, S., Takemura, T., Chikira, M., Ogura, T., Sekiguchi, M., Takata, K., Yamazaki, D., Yokohata, T., Nozawa, T., Hasumi, H., Tatebe, H., and Kimoto, M.: Improved climate simulation by MIROC5: mean states, variability, and climate sensitivity, *J. Climate*, 23, 6312–6335, 2010.
- 20 Watanabe, S., Hajima, T., Sudo, K., Nagashima, T., Takemura, T., Okajima, H., Nozawa, T., Kawase, H., Abe, M., Yokohata, T., Ise, T., Sato, H., Kato, E., Takata, K., Emori, S., and Kawamiya, M.: MIROC-ESM: model description and basic results of CMIP5-20c3m experiments, *Geosci. Model Dev. Discuss.*, 4, 1063–1128, doi:10.5194/gmdd-4-1063-2011, 2011.
- 25 Wientjes, I. G. M. and Oerlemans, J.: An explanation for the dark region in the western melt zone of the Greenland ice sheet, *The Cryosphere*, 4, 261–268, doi:10.5194/tc-4-261-2010, 2010.
- 30 Wientjes, I. G. M., Van de Wal, R. S. W., Reichart, G. J., Sluijs, A., and Oerlemans, J.: Dust from the dark region in the western ablation zone of the Greenland ice sheet, *The Cryosphere*, 5, 589–601, doi:10.5194/tc-5-589-2011, 2011.

Xing, J., Pleim, J., Mathur, R., Pouliot, G., Hogrefe, C., Gan, C.-M., and Wei, C.: Historical gaseous and primary aerosol emissions in the United States from 1990 to 2010, *Atmos. Chem. Phys.*, 13, 7531–7549, doi:10.5194/acp-13-7531-2013, 2013.

5 Xing, J., Mathur, R., Pleim, J., Hogrefe, C., Gan, C.-M., Wong, D. C., Wei, C., Gilliam, R., and Pouliot, G.: Observations and modeling of air quality trends over 1990–2010 across the Northern Hemisphere: China, the United States and Europe, *Atmos. Chem. Phys.*, 15, 2723–2747, doi:10.5194/acp-15-2723-2015, 2015.

The darkening of the Greenland ice sheet

M. Tedesco et al.

Title Page

Abstract

Introduction

Conclusions

References

Tables

Figures



Back

Close

Full Screen / Esc

Printer-friendly Version

Interactive Discussion



The darkening of the Greenland ice sheet

M. Tedesco et al.

Title Page

Abstract

Introduction

Conclusions

References

Tables

Figures

◀

▶

◀

▶

Back

Close

Full Screen / Esc

Printer-friendly Version

Interactive Discussion



Table 2. June–July–August mean and standard deviation of measured aerosol optical depth (AOD) at 550 nm at the three sites of Thule, Ittoqqortoormiit and Kangerlussuaq of the AERONET network (AERONET web site, <http://aeronet.gsfc.nasa.gov>, 2013).

| Year | Station | | |
|------|--------------------------------------|---|--|
| | Thule 77°28′00″ N, 69°13′50″ W | Ittoqqortoormiit 70°29′07″ N, 21°58′00″ W | Kangerlussuaq 67°00′31″ N, 50°41′21″ W |
| 2007 | 0.042 ± 0.010 | NA | NA |
| 2008 | 0.040 ± 0.017 | NA | 0.051 ± 0.012 |
| 2009 | 0.093 ± 0.020 | NA | 0.088 ± 0.017 |
| 2010 | 0.052 ± 0.011 | 0.052 ± 0.005 | 0.049 ± 0.007 |
| 2011 | 0.060 ± 0.017 | 0.072 ± 0.041 | 0.053 ± 0.012 |
| 2012 | 0.065 ± 0.011 | 0.044 ± 0.009 | 0.072 ± 0.020 |
| 2013 | 0.050 ± 0.007 | 0.053 ± 0.009 | 0.066 ± 0.010 |

The darkening of the Greenland ice sheet

M. Tedesco et al.

Title Page

Abstract

Introduction

Conclusions

References

Tables

Figures

◀

▶

◀

▶

Back

Close

Full Screen / Esc

Printer-friendly Version

Interactive Discussion



Table 3. Mean, standard deviation and maximum absolute difference of the difference between grain size in the case of pure snow and in the case of snow with impurities that reduce visible-band albedo by 0.01, 0.03 and 0.05. The difference is expressed as a percentage relative to the grain size value obtained in the case of pure snow.

| Grain size difference [%] | $\Delta\alpha$ | | |
|-----------------------------|----------------|-------|-------|
| | −0.01 | −0.03 | −0.05 |
| Mean | 1.01 | 1.22 | 1.12 |
| Standard deviation | 1.88 | 3.22 | 2.42 |
| Maximum absolute difference | 20.3 | 22.1 | 16.3 |

The darkening of the Greenland ice sheet

M. Tedesco et al.

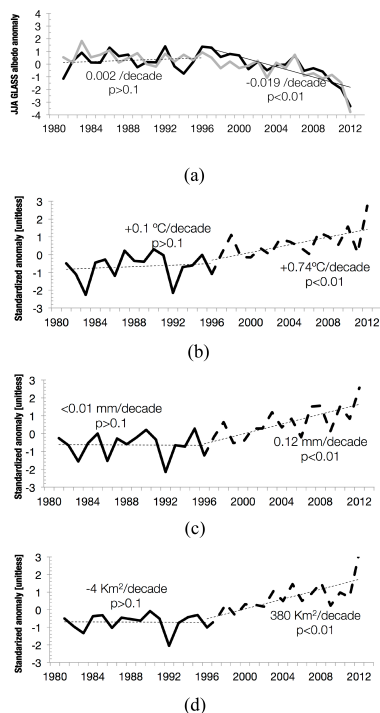


Figure 1. Mean summer standardized values plotted as time series for **(a)** albedo from GLASS (black) and MAR (grey), together with MAR-simulated values of **(b)** surface air temperature, **(c)** surface grain size (effective radius of optically “equivalent” sphere) and **(d)** bare ice exposed area. Trends for the periods 1981–1996 and 1996–2012 are reported in each plot. Trends in **(a)** refer to the GLASS albedo. The baseline 1981–2012 period is used to compute standardized anomalies, obtained by subtracting the mean and then dividing by the standard deviation of the values in the time series. All trends are computed from JJA averaged values over ice-covered areas only, not tundra.



Full Screen / Esc

Abstract

Introduction

Conclusions

References

Tables

Figures



Back

Close

Printer-friendly Version

Interactive Discussion

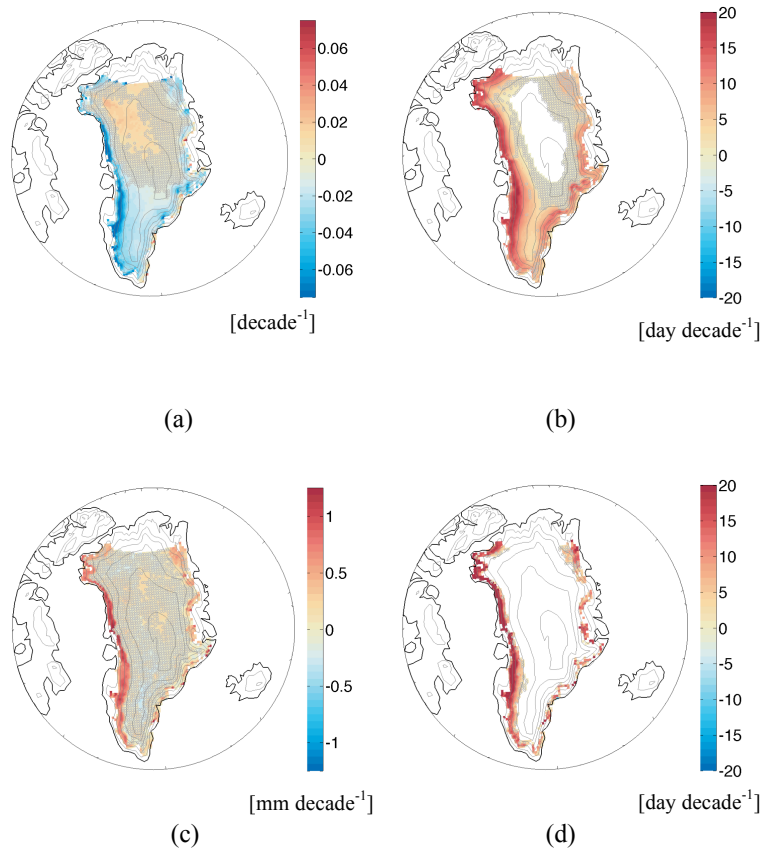


Figure 2. Maps of JJA trends (per decade) from 1996 to 2012, when darkening began to occur, for **(a)** GLASS albedo, **(b)** number of days when surface air temperature exceeded 0°C , **(c)** surface grain size and **(d)** number of days when bare ice is exposed. Regions where trends are not significant at a 95 % level are shown as grey-hatched areas. White regions over the north end of the ice sheet indicate areas or were not viewed by the satellite.

The darkening of the Greenland ice sheet

M. Tedesco et al.

Title Page

Abstract Introduction

Conclusions References

Tables Figures

◀ ▶

◀ ▶

Back Close

Full Screen / Esc

Printer-friendly Version

Interactive Discussion



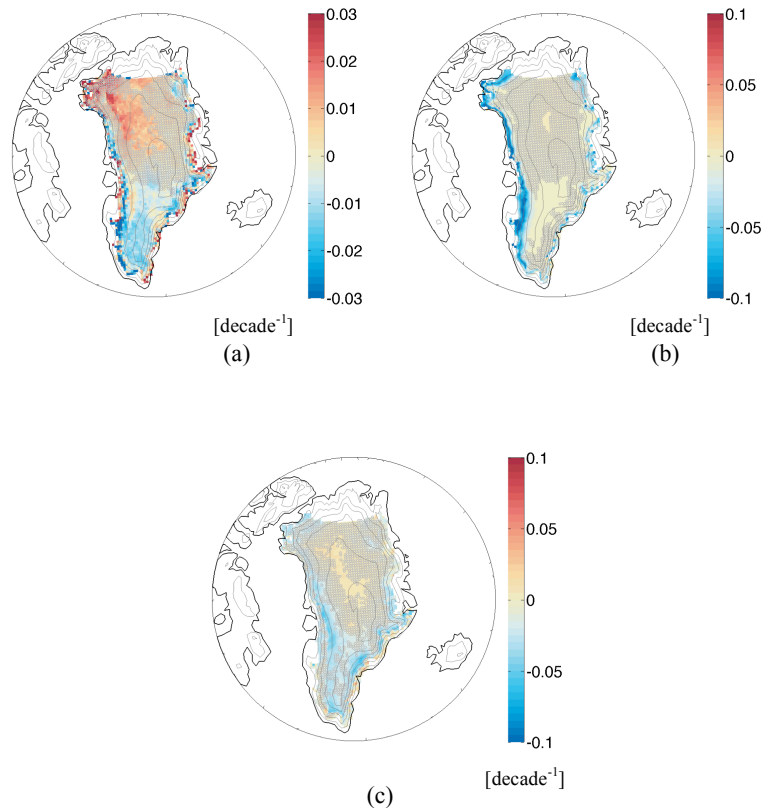


Figure 3. Differences between spaceborne measured and model-simulated albedo trends in different spectral regions. **(a)** Difference between the MAR and GLASS trends (albedo change per decade), with positive values indicating those regions where MAR trend is smaller in magnitude than GLASS. Maps of JJA mean albedo trends (1996–2012) simulated by MAR for **(b)** visible and **(c)** near-infrared wavelengths.

The darkening of the Greenland ice sheet

M. Tedesco et al.

| | |
|--------------------------|--------------|
| Title Page | |
| Abstract | Introduction |
| Conclusions | References |
| Tables | Figures |
| ◀ | ▶ |
| ◀ | ▶ |
| Back | Close |
| Full Screen / Esc | |
| Printer-friendly Version | |
| Interactive Discussion | |



The darkening of the Greenland ice sheet

M. Tedesco et al.

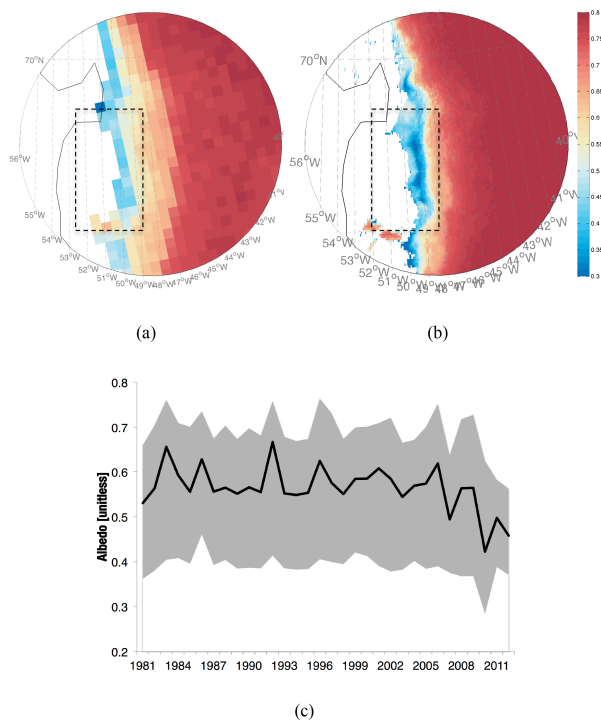


Figure 4. (a) MAR and (b) GLASS mean JJA albedo for year 2010 over an area including the dark band together with (c) time series of mean JJA albedo for the ice-covered areas in the black rectangle. The black line in (c) shows the GLASS spatially averaged albedo, where the top and the bottom of the grey area indicate, respectively, the maximum and minimum albedo within the black box in (b).

The darkening of the Greenland ice sheet

M. Tedesco et al.

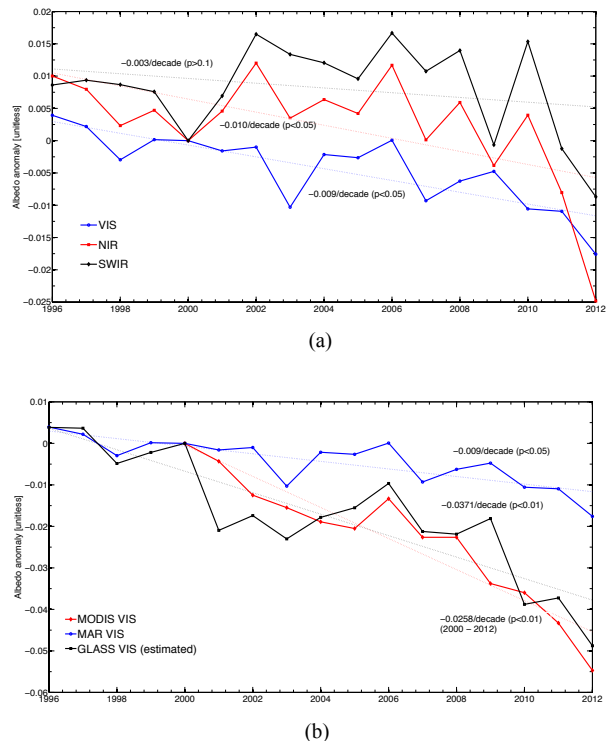


Figure 5. Time series of modelled and measured mean summer (JJA) albedo anomalies (with respect to year 2000) in different spectral bands. **(a)** Visible, near-infrared and shortwave-infrared albedo values simulated by MAR; **(b)** as in **(a)** but for the visible albedo only for MAR, MODIS (obtained from the product MCD43) and GLASS. Note that the vertical axis scale in **(b)** is different from that in **(a)**.

Title Page

Abstract

Introduction

Conclusions

References

Tables

Figures



Back

Close

Full Screen / Esc

Printer-friendly Version

Interactive Discussion



The darkening of the
Greenland ice sheet

M. Tedesco et al.

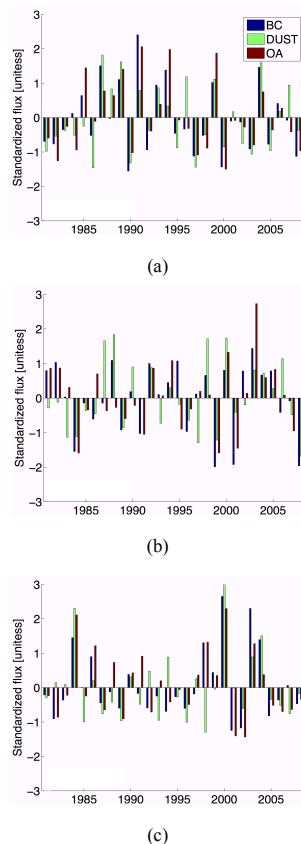
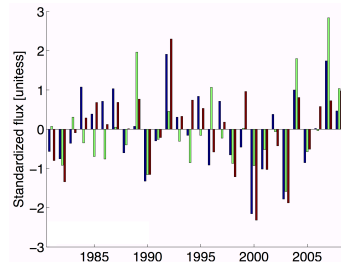
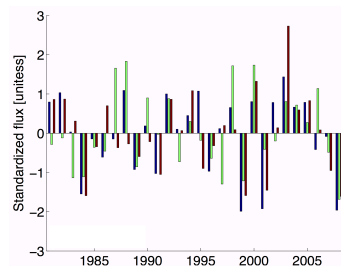


Figure 6. AEROCOM standardized deposition fluxes for BC, dust and organic aerosol at Kangerlussuaq for **(a)** June, **(b)** July and **(c)** August (1981–2008).

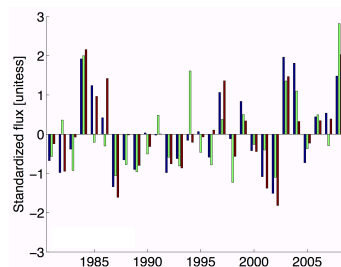
[Title Page](#)[Abstract](#)[Introduction](#)[Conclusions](#)[References](#)[Tables](#)[Figures](#)[I◀](#)[▶I](#)[◀](#)[▶](#)[Back](#)[Close](#)[Full Screen / Esc](#)[Printer-friendly Version](#)[Interactive Discussion](#)



(a)



(b)



(c)

Figure 7. Same as Fig. 6 but for Summit station.

The darkening of the Greenland ice sheet

M. Tedesco et al.

| | |
|--------------------------|--------------|
| Title Page | |
| Abstract | Introduction |
| Conclusions | References |
| Tables | Figures |
| ◀ | ▶ |
| ◀ | ▶ |
| Back | Close |
| Full Screen / Esc | |
| Printer-friendly Version | |
| Interactive Discussion | |



The darkening of the Greenland ice sheet

M. Tedesco et al.

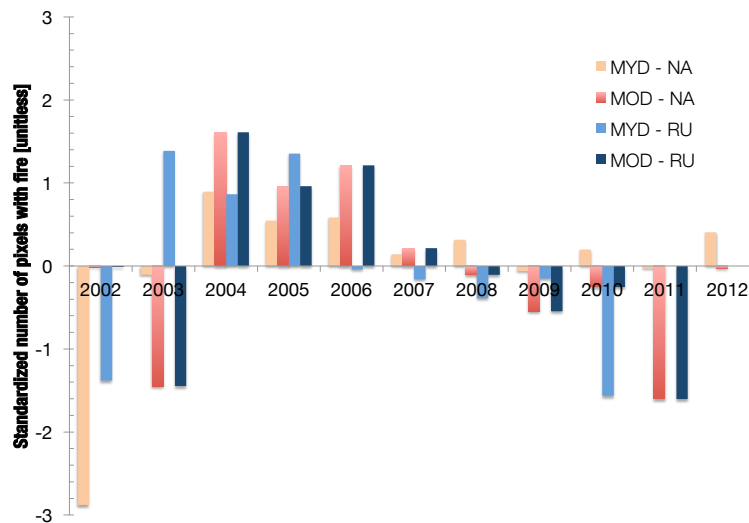


Figure 8. Standardized cumulative number of fires detected over North America and Eurasia by the MOD14CMH and MYD14CMH GCM climatology products between 2002 and 2012.

| | |
|--------------------------|--------------|
| Title Page | |
| Abstract | Introduction |
| Conclusions | References |
| Tables | Figures |
| ◀ | ▶ |
| ◀ | ▶ |
| Back | Close |
| Full Screen / Esc | |
| Printer-friendly Version | |
| Interactive Discussion | |



The darkening of the Greenland ice sheet

M. Tedesco et al.

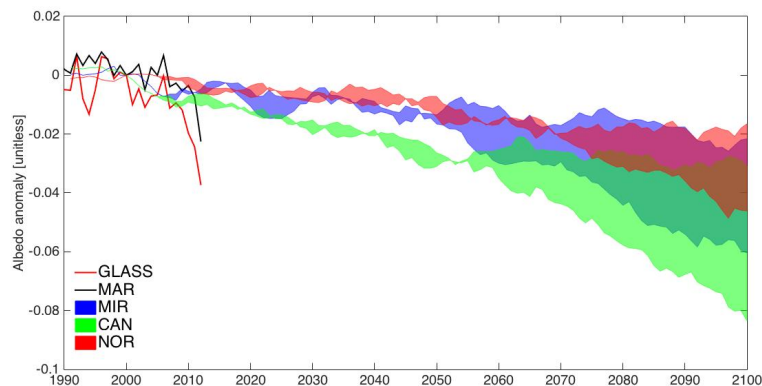


Figure 9. Projections of broadband albedo anomaly (with respect to year 2000) averaged over the whole GIS for 1990–2012 from MAR simulations and GLASS retrievals (black and red lines, respectively), and as projected by 2100. Future projections are simulated with MAR forced at its boundaries with the outputs of three ESMs under two warming scenarios, with the first scenario (RCP45) corresponding to an increase in the atmospheric greenhouse gas concentration to a level of 850 ppm CO₂ equivalent by 2100 and the second (RCP85) to > 1370 ppm CO₂ equivalent. The top and the bottom of the coloured area plots represent the results concerning the RCP45 (bottom) and RCP85 (top) scenarios. Semi-transparent colours are used to allow view of the overlapping data. Dark green corresponds to the case where MIROC5 and CANESM2 results overlap and brown to the case when the results from the three ESMs overlap.

Title Page

Abstract

Introduction

Conclusions

References

Tables

Figures



Back

Close

Full Screen / Esc

Printer-friendly Version

Interactive Discussion



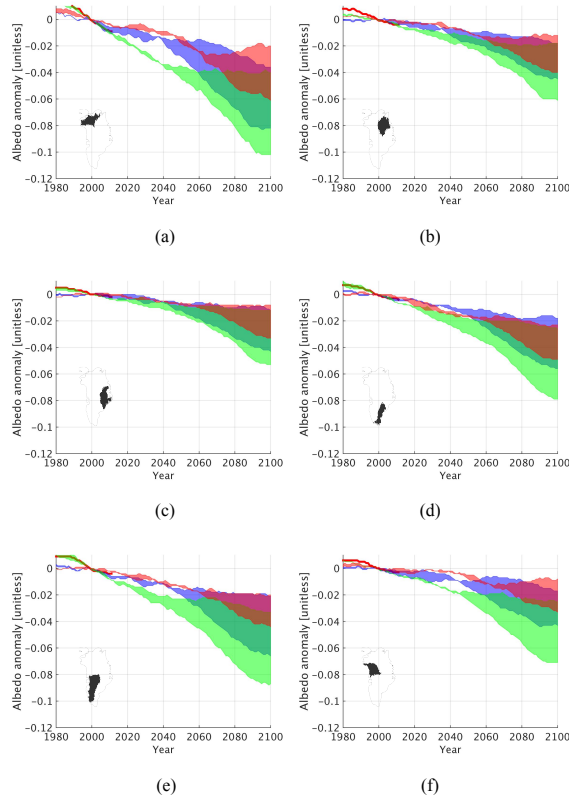
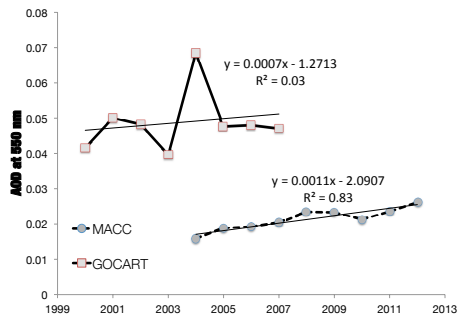


Figure 10. Same as Fig. 9 but for different drainage regions of the GrIS, indicated by the small maps in each panel. Dark grey corresponds to MIROC5 simulations, mild grey to CanESM and light grey to NORESM. The top and the bottom of each area plots represent the results concerning the RCP45 (bottom) and RCP85 (top) scenarios. Red lines represent the GLASS albedo averaged over the corresponding drainage region.

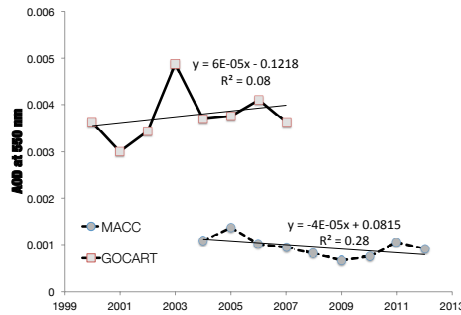


WARMING-DRIVEN DARKENING OF THE GREENLAND ICE SHEET

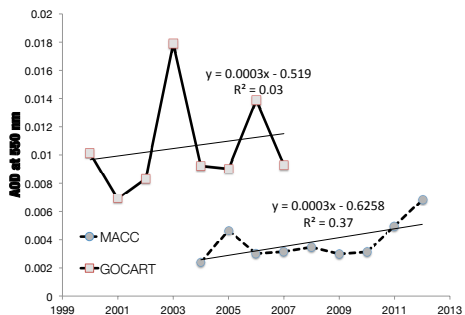


(a)

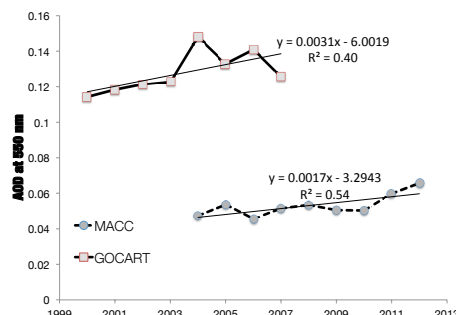
WARMING-DRIVEN DARKENING OF THE GREENLAND ICE SHEET



(c)



(b)

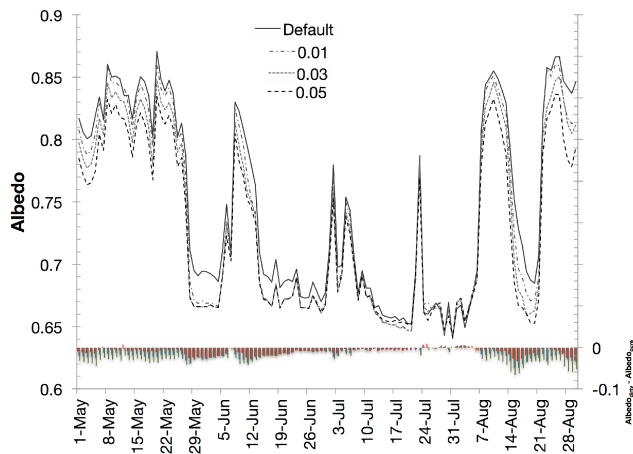


(d)

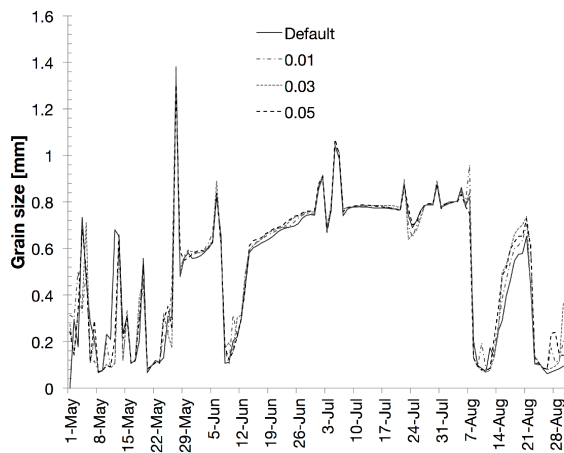
Figure 11. May–June averaged aerosol optical depth at 550 nm for **(a)** dust, **(b)** organic matter, **(c)** black carbon and **(d)** total obtained from the GOCART model and from the MACC model (as in Dumont et al., 2014) for the domain bounded by 75–80° N and 30–50° W.

The darkening of the Greenland ice sheet

M. Tedesco et al.



(a)



(b)

| | |
|--------------------------|--------------|
| Title Page | |
| Abstract | Introduction |
| Conclusions | References |
| Tables | Figures |
| ◀ | ▶ |
| ◀ | ▶ |
| Back | Close |
| Full Screen / Esc | |
| Printer-friendly Version | |
| Interactive Discussion | |



Figure 12. (a) Daily broadband albedo and **(b)** grain size simulated by MAR over a $100 \times 100 \text{ km}^2$ area centred at Swiss Camp obtained when MAR simulated visible-band albedo is reduced by 0.01, 0.03 and 0.05 to simulate the effects of light-absorbing impurities in snow. The default value refers to the albedo calculated for impurity-free snow (Eq. 2). Bars at the bottom of plot **(a)** (right-hand y axis) gives the difference between the albedo of pure snow (“default”) and that when visible albedo is reduced (i.e., dirty snow).

The darkening of the Greenland ice sheet

M. Tedesco et al.

Title Page

Abstract

Introduction

Conclusions

References

Tables

Figures



Back

Close

Full Screen / Esc

Printer-friendly Version

Interactive Discussion

